Universiteit Leiden
The Netherlands

Nanoplastics causes extensive congenital malformations during embryonic development by passively targeting neural crest cells

Wang, M.; Rücklin, M.; Poelmann, R.E.; Mooij, C.L. de; Fokkema, M.; Lamers, G.E.M.; ... ; Richardson, M.K.

Citation
Wang, M., Rücklin, M., Poelmann, R. E., Mooij, C. L. de, Fokkema, M., Lamers, G. E. M., … Richardson, M. K. (2023). Nanoplastics causes extensive congenital malformations during embryonic development by passively targeting neural crest cells. *Environment International*, *173*. doi:10.1016/j.envint.2023.107865

Version:	Publisher's Version
License:	Creative Commons CC BY 4.0 license
Downloaded from:	https://hdl.handle.net/1887/3571021

Note: To cite this publication please use the final published version (if applicable).

Environment International 173 (2023) 107865

Contents lists available at ScienceDirect

Environment International

journal homepage: www.elsevier.com/locate/envint

Full length article

Nanoplastics causes extensive congenital malformations during embryonic development by passively targeting neural crest cells

Meiru Wang [a,b], Martin Rücklin [a,b], Robert E. Poelmann [a,c], Carmen L. de Mooij [a], Marjolein Fokkema [d], Gerda E.M. Lamers [a], Merijn A.G. de Bakker [a], Ernest Chin [a], Lilla J. Bakos [a], Federica Marone [e], Bert J. Wisse [f], Marco C. de Ruiter [f], Shixiong Cheng [a], Luthfi Nurhidayat [a,g], Martina G. Vijver [h], Michael K. Richardson [a,*]

[a] Institute of Biology, Leiden University, Sylvius Laboratory, Sylviusweg 72, 2333 BE Leiden, The Netherlands
[b] Naturalis Biodiversity Center, Darwinweg 2, 2333 CR Leiden, The Netherlands
[c] Department of Cardiology, Leiden University Medical Center, The Netherlands
[d] Institute of Psychology, Methodology and Statistics, Pieter de la Court Building, Wassenaarseweg 52, 2333 AK Leiden, The Netherlands
[e] Swiss Light Source, Paul Scherrer Institut, Photon Science Department, Forschungsstrasse 111, CH-5232 Villigen, Switzerland
[f] Department of Anatomy & Embryology, Leiden University Medical Center, The Netherlands
[g] Faculty of Biology, Universitas Gadjah Mada, Yogyakarta, Indonesia
[h] Institute of Environmental Sciences, Leiden University (CML), Van Steenis Building, Einsteinweg 2, 2333 CC Leiden, The Netherlands

ARTICLE INFO

Handling Editor: Adrian Covaci

Keywords:
Nanoplastics
Congenital malformation
Neural crest
Neural tube defects
Cardiac malformations

ABSTRACT

Nanomaterials are widespread in the human environment as pollutants, and are being actively developed for use in human medicine. We have investigated how the size and dose of polystyrene nanoparticles affects malformations in chicken embryos, and have characterized the mechanisms by which they interfere with normal development. We find that nanoplastics can cross the embryonic gut wall. When injected into the vitelline vein, nanoplastics become distributed in the circulation to multiple organs. We find that the exposure of embryos to polystyrene nanoparticles produces malformations that are far more serious and extensive than has been previously reported. These malformations include major congenital heart defects that impair cardiac function. We show that the mechanism of toxicity is the selective binding of polystyrene nanoplastics nanoparticles to neural crest cells, leading to the death and impaired migration of those cells. Consistent with our new model, most of the malformations seen in this study are in organs that depend for their normal development on neural crest cells. These results are a matter of concern given the large and growing burden of nanoplastics in the environment. Our findings suggest that nanoplastics may pose a health risk to the developing embryo.

1. Introduction

Plastics are polymer-based materials made of synthetic or semi-synthetic organic compounds and derived from petroleum products (Desai and Galage 2015). They are durable, cheap, water-resistant, have relatively low energy requirements for their manufacture, and are relatively light in weight (Panda et al. 2010). Moreover, plastics can be significantly altered by heating (Levine and Berman 1995). Therefore, plastics have a broad range of applications in manufacturing, the electronics, packaging and food industries, and in agriculture and medicine and surgery (Gourmelon 2015). Since the 1950s, the annual global growth rate in plastics production has remained at an average of 8.5 % (Platt 2003). By 2018, global plastics production reached 359 million metric tonnes. According to some predictions, this value will have doubled by 2025 (Gibb 2019).

Plastics have become a large component of domestic garbage and industrial waste (Subramanian 2000). In addition, this plastic waste can persist for years in the environment due to the low speed at which plastics undergo degradation (Webb et al. 2012). Plastic waste can been found in freshwater bodies, oceans, soil, air, and even in remote, uninhabited islands (Bergmann et al. 2019). For these reasons, plastic pollution in our environment is a matter for great concern (Boehnke et al. 2022; Chauhan and Wani 2019).

Microplastics and nanoplastics (MPs and NPs) are small plastic

* Corresponding author.
E-mail address: m.k.richardson@biology.leidenuniv.nl (M.K. Richardson).

https://doi.org/10.1016/j.envint.2023.107865
Received 3 January 2023; Received in revised form 30 January 2023; Accepted 3 March 2023
Available online 6 March 2023
0160-4120/© 2023 The Authors. Published by Elsevier Ltd. This is an open access article under the CC BY license (http://creativecommons.org/licenses/by/4.0/).

particles with relevance to human health. They are being considered as new drug delivery vehicles for use in human medicine (Boehnke et al. 2022). Furthermore, MPs and NPs are widely distributed as pollutants in the environment (Auta et al. 2017; Ball 2021; Koelmans et al. 2019; Vighi et al. 2021; Zhang et al. 2020). A distinction can be made between primary small plastic particles, which are manufactured as such; and secondary small plastic particles which arise from the break-down in the environment of larger pieces of plastic (Bradney et al. 2019). Furthermore, it is important to note that the toxicity of nanoplastics can, in principle, be due to their properties as polymers, or to the toxicity of additives used during manufacture (Sridharan et al. 2022).

The potentially harmful effects of and MPs and NPs have mostly been studied in aquatic organisms including crustaceans (e.g. *Daphnia magna*), gastropods, and fish (e.g. zebrafish; (Kögel et al. 2020). These studies have shown that MPs and NPs can produce a range of toxic effects including: growth delays, development toxicity, behavioural abnormalities and metabolic effects (Brun et al. 2019), and bradycardia (Kögel et al. 2020). In mammals, MPs and NPs can have deleterious effects on the immune and nervous systems, and on metabolism (Yong et al., 2020). It has also been shown that polystyrene nanoparticles (PS-NPs) can cause neural tube and craniofacial defects in chick embryos; the neural tube defects in that study were attributed to the induction of apoptosis in the neural tube (Nie et al. 2021).

Our aims here are as follows: (i) to unravel the action of PS-NPs on warm-blooded vertebrate embryos. We have used the chick embryo as a model (Butler et al. 2022; Geetha-Loganathan et al., 2011; Kohl et al. 2019); (ii) to provide a detailed phenotypic analsysis of the malformations induced in this speices by PS-NPs; (iii) to identify the localisation of fluorescent PS-NPs in the chicken embryo; (iv) to identify cell populations affected by PS-NPs by using molecular markers. Our hypothesis driving this study is that PS-NPs have a deleterious effect by damaging a specific subpopulation of embryonic cells. We find that phenotypic analysis of the treated embryos reveals a much wider range of congenital malformations than previously reported — including heart defects, which have not been described in the context of NP exposure before. Our molecular and cellular analyses show that most of the malformations can be explained by a highly selective effect of PS-NPs on neural crest cells, an embryonic population of migratory stem cells.

2. Materials and methods

2.1. Preparation and analysis of nanoplastics

2.1.1. Plain 25 nm polystyrene nanoplastics

Sterile, plain (non-functionalized) polystyrene nanoplastics (PS-NPs) were purchased from Lab 261 (cat. number PST25, Palo Alto, U.S.), with nominal diameter of 25 nm (1 % solid, 1.05 g/cm^3). As supplied by the manufacturer, the PS-NP suspension was in a vehicle of 0.03 % Tween®20 in Milli-Q® water. We specifically requested the manufacture to not add azide. The suspension was then diluted with Ringer's solution (pH 7, 2.5 g/L, cat. number 1.15525, Merck Millipore, Germany), which we autoclaved before use. The dilution series in Ringer's was as follows: 2, 10, 100, and 1000 × to yield final PS-NP concentrations of 5 mg/ml, 1 mg/ml, 0.1 mg/ml, and 0.01 mg/ml, respectively.

The sterility of the PS-NPs suspensions was tested by streaking on LB agar plates (File S1). PS-NP size, shape and zeta-potential in Milli-Q® water or Ringer's solution were measured by multi angle dynamic light scattering (MADLS; Malvern Panalytical ltd., Malvern, UK) and TEM (transmission electron microscopy using a JEOL 1400 +). The suspensions were sonicated for 10 min before use using a USC200T ultrasonic cleaning bath (VWR, Amsterdam, the Netherlands).

2.1.2. Fluorescent 25 nm polystyrene nanoplastics

Fluorescent (non-functionalized) nanoparticles (nominal diameter 25 nm) were also obtained on special request from the manufacturer (Lab 261), without azide added. They were green fluorescent polystyrene nanoparticles (cat. number FGP25; 1 % solid, 1.05 g/cm^3). They were further handled and characterised as described for the plain PS-NPs.

2.1.3. Fluorescent carboxylate-modified 500 nm and 1 μm polystyrene nanoparticles

We used (i) fluorescent, carboxylate-modified polystyrene particles with a nominal diameter of 500 nm (red fluorescence, 2 % solid, 1.055 g/cm^3; Invitrogen™, cat. number F8813) and (ii) fluorescent, carboxylate-modified polystyrene particles with a nominal diameter of 1 μm, (green fluorescence, 2 % solid, 1.055 g/cm^3; Invitrogen™, cat. number F8823). The products as supplied were sonicated by us for 10 min using a USC200T ultrasonic cleaning bath (VWR, Amsterdam, the Netherlands) then diluted with Ringer's solution to a final concentration of 0.1 mg/ml or 0.01 mg/ml, respectively. They were sonicated again for 10 min before use.

2.2. In ovo embryo toxicity experiments

Fertilised eggs of the White Leghorn chicken (*Gallus gallus*) strain were purchased from a commercial supplier (Drost Loosdrecht B.V., the Netherlands). They were incubated for 29 h at 38 °C on stationary shelves in a humidified, forced-draft incubator (Binder, Germany). Under aseptic conditions, the eggs were windowed and staged as described in Ref. (Hamburger and Hamilton 1951). Then, 50 μL Ringers' solution was dripped onto the dorsal side of the embryo to moisten the vitelline membrane. Next, a small hole was made in the vitelline membrane using a sharpened tungsten needle (Brady 1965; Silver 1960). It was made beyond the head of the embryo, avoiding the embryo itself. Next, 50 μL of either (i) working solutions of PS-NPs or (ii) Ringer's solution as a vehicle-only control, was dripped onto the hole using a Gilson P200 Pipetman®. The egg was then sealed with Scotch® prescription label tape 800 (clear) and returned to the incubator for 24 h, 4 d or 8 d. Finally, embryos were harvested into cold phosphate buffered saline (PBS).

2.3. Heart-rate recordings and analysis

The 2 dpe and 3 dpe chick embryos were placed, still in the egg, in a cradle of crumpled aluminium foil in a digital heat block (38 °C). Video recordings were made of the embryo *in ovo* using a Nikon SMZ800 stereo microscope fitted with a Dino-Eye eyepiece camera (Dino-Lite Europe, Almere). To determine the heart rate of chicken embryos, 27 videos were analysed using ImageJ (v. 1.53q Java 1.8.0_322, National Institutes of Health, USA) and a custom script written by Joost Willemse. Videos were made into an image stack. Then, an area of the heart was selected using the rectangle tool so that the heart beat would be registered by a change in colour. The mean grey value of the selected area was calculated for each frame of the video.

2.4. In ovo injections

2.4.1. Sub-blastodermic injections

Stage 16–17 chicken embryos were injected with 200 μL of 500 nm red fluorescent carboxyl-modified polystyrene particle suspension (or Ringer's solution only for vehicle-only controls). The injections were made into the sub-blastodermal space using a 28G hypodermic needle and each took c. 5 s. The embryos were then sealed and incubated for a further 2 days.

2.4.2. Vitelline vein injections

Stage 18–19 chicken embryos were injected with 5 μL of a suspension of 1 μm green fluorescent carboxyl-modified polystyrene particles (or Ringer's solution only) were injected into the vitelline vein. Each injection took c. 2.5 min in total. We used Harvard glass needles (GC100F-10) pulled with a Flaming/Brown micropipette puller (Sutter

Instruments Model P-87). The needles were mounted on a Leitz micromanipulator. The pressure of the injections was generated with a Picospritzer III (Parker Hannifin Corp.) with the pulse duration set at 15–25 ms.

2.4.3. Analysis of injected embryos

After further incubation (see above), injected embryos were analysed as follows (i) videos were made of the living embryos under light from an SFA fluorescence excitation light (Nightsea, Hatfield, PA) with a Nightsea SFA yellow barrier filter in front of the microscope objective, and (ii) embryos were fixed in 4 % buffered depolymerised paraformaldehyde (pFA) for 24 h at 4 °C and photographed.

2.5. Alcian blue wholemounts

This protocol is as previously described by us (de Bakker et al., 2013). Embryos were fixed with 5 % trichloroacetic acid at 4 °C degree overnight. They were then transferred into refresh 70 % ethanol for 2 h × 2 followed by acid alcohol (20 % glacial acetic acid in 70 % ethanol for 2 h). Embryos were then stained in 0.03 % (W/V) Alcian blue in acid alcohol overnight. Then they were rinsed with acid alcohol for 2 h followed by dehydration through a graded ethanol series from 70 % to 100 %. Finally, embryos were cleared and stored in methyl salicylate.

2.6. Histology

We performed routine paraffin histology with haematoxylin and eosin staining according to standard protocols (Bancroft and Gamble, 2008). Embryos were fixed in 4 % buffered depolymerised paraformaldehyde (pFA) for 24 h at 4 °C. They were then were washed 3x with cold PBS and dehydrated in 70 % ethanol overnight. Subsequently, the embryos were dehydrated through a graded ethanol series (80 %, 90 %, 100 %), 1 h each. Embryos were cleared with NeoClear® (Merck, Darmstadt), 3x 1 h, and embedded in paraffin (Paraclean, KP Klinipath/VWR International, Amsterdam) at 60 °C (1x overnight, 1x 1 h). Sections were cut at 7 μm. Because embryos examined at 24 h post-exposure were delicate and difficult to handle, we used a modified protocol (McClelland et al., 2016). After fixing the embryos, they were embedded in a mixture of 2 % agarose (Sigma-Aldrich, Zwijndrecht, A-6013) and 2.5 % low melting-point agarose (super fine resolution agarose, Electron Microscopy Sciences, Hatfield, PA) at 42 °C. When the mixture had solidified at room temperature (c. 20 min), the agarose blocks containing the embedded embryos were transferred to 70 % ethanol for 2 d. They were then dehydrated in graded ethanols, embedded in paraffin and sectioned. The only modification made to the embedding step was that the tissue blocks were in molten paraffin for nomore than 3 × 1 h.

2.7. MicroCT

This protocol for X-ray microtomography (microCT; Refs. (Metscher 2009)) was described previously by us (Yi et al. 2021). In brief, embryos were fixed in 4 % pFA in PBS (pH 7.4) at 4 °C for 24 h. They were then rinsed 3 × with PBS, 4 °C. After dehydration in a graded ethanol series (25 %, 50 %, 70 %) they were stained with phosphotungstic acid (0.3 % in 70 % ethanol) for 48 h on a rotary shaker. After staining, embryos were stored in 70 % ethanol. For scanning, embryos were immobilised in 1 % low melting-point agarose in 1 ml pipette tips, and sealed with parafilm. For scan parameters, see Table S1. The images were analysed and manipulated using Avizo software (Version: 8.01; Thermo, Fisher Scientific).

2.8. Synchrotron X-ray tomographic microscopy

For synchrotron X-ray tomographic microscopy (synchrotron scanning) embryos were harvested and fixed in a mixture of 2.5 % pFA, 1.5 % glutaraldehyde in 0.1 M sodium cacodylate buffer (pH 7.4) at 4° C for 24 h as previously described (Cotti et al. 2020). They were then dehydrated in a graded ethanol series. The hearts were dissected and stored in 0.2 ml PCR tubes in 70 % ethanol at 4 °C. X-ray tomographic microscopy was performed at the TOMCAT beamline (Stampanoni et al. 2006), at the Swiss Light Source, Paul Scherrer Institute, Villigen, Switzerland). The samples were fixed to scanning electron microscopy stubs with beeswax. The X-ray beam energy was 17 keV. For the overview scans, the microscope (Optique Peter, Lentilly, France) magnification was set to 4x. To be able to laterally cover the entire sample, the rotation axis was displaced to the side of the field of view and 2,501 projections, equiangularly distributed over 360°, were acquired with a sCMOS camera (PCO.edge, Kehlheim, Germany). To fully cover the sample in the vertical direction, a sequence of 3–4 scans was necessary. The exposure time per projection was 50 ms and the X-rays were converted into visible light with a 100 μm thick Ce doped LuAG scintillator screen (Crytur, Turnov, Czech Republic). The effective pixel size was 1.625 μm and the sample-detector distance 20 cm. For the higher resolution scans of specific details, a 10x objective with a thinner (20 μm) scintillator of the same material was used, resulting in a pixel size of 0.65 μm. The rotation axis was positioned in the middle of the field of view, and 1,501 projections, equiangularly distributed over 180°, were acquired with an exposure time per view of 200 ms. Prior to tomographic reconstruction (Marone et al. 2017), all projections were dark- and flat-field corrected as well as phase-retrieved (Paganin et al. 2002). The images were analysed and manipulated using Avizo software (Version: 8.01; Thermo, Fisher Scientific).

2.9. Localisation of fluorescent 25 nm PS-NPs in ovo and in vitro

Chicken embryos were exposed to PS-NPs as described above under '*In ovo* embryo toxicity experiments' with the exception that instead of plain PS-NPs, we used green fluorescent polystyrene nanoparticles (cat. number FGP25; 1 % solid, 1.05 g/cm^3). The embryos were returned to the incubator and re-incubated for 2, 6 and 24 h. They were then removed from the egg and visualised as wholemounts by confocal microscopy (Zeiss Airyscan 900); or after sectioning with a cryostat (Leica CM3050S) and imaging with a Zeiss Axioplan 2 fluorescence microscope.

For neural crest and somite cell cultures, Hamburger-Hamilton (Hamburger and Hamilton 1951) stage 14–15 embryos were removed from the egg, and rinsed with sterile calcium-magnesium free Dulbecco's PBS (CMF; Corning®, New York). The method of Cohen and Konigsberg was used, slightly modified (Cohen and Konigsberg 1975). In brief, a segment of the embryo body from the axial levels of the last 6–9 somites was cut out using tungsten needles and placed in 0.25 % Trypsin-EDTA (Sigma-Aldrich, Zwijndrecht, T4049) on ice for 8–10 min, when the somites and neural tube appeared to be beginning to separate from the surrounding tissues. The segments were then transferred to DMEM (Sigma-Aldrich, Zwijndrecht, D0819) 15 % foetal calf serum (Sigma-Aldrich, Zwijndrecht, F7524) and 1 % antibiotic–antimycotic (Sigma-Aldrich, Zwijndrecht, A5955).

The tissue pieces were gently triturated with a blue Gilson pipette tip (with the tip cut off and the cut surface polished in a flame). Then, neural tubes and somites were plated into separate culture dishes containing culture medium (MEM, HEPES, GlutaMAX™ Supplement (42360, Gibco™ with 15 % foetal calf serum and 1 % antibiotic–antimycotic). Most of the medium was then aspirated leaving the tissue samples pressed against the substratum by surface tension. They were incubated for 4 h or until attached and then 1 ml culture medium was added. They were cultured overnight in a 5 % CO_2 incubator (37 °C). The culture dishes were *μ-Dish* 35 mm high glass-bottom dishes (ibidi GmbH; Gräfelfing, Germany) which we pre-coated with rat-tail collagen type-I (cat. number 50201), also from ibidi, according to the manufacturer's instructions.

We exposed 2 d cultures of chick neural crest to 1 ml of 0.1 mg/mL fluorescent PS-NPs (25 nm) for either 2 h or 6 h. Cultures were then

rinsed 3 × with warm culture medium and stained with 5 μg/mL DAPI (4′,6-diamidino-2-phenylindole; Invitrogen™) in culture medium for 20 min at 37 °C. The cultures were rinsed with fresh medium only and observed under a Zeiss Airyscan 900 confocal microscope.

2.10. Cryosections

Embryos were fixed with 4 % pFA in PBS and then transferred to 30 % sucrose solution in PBS (4 h, 4 °C). They were then transferred to OCT embedding matrix (Carl Roth, Karlsruhe) 1 × 1 h (4 °C) then transferred to fresh OCT in a plastic mould and snap frozen in liquid nitrogen. Sections were cut at 25 μm using a Leica CM3050S cryostat and mounted on glass microscope slides. The slides were analysed using Zeiss Axioplan 2 aka DIC.

2.11. Wholemount in situ hybridization

In this study, all gene names are according to Ensembl for *Homo sapiens* (https://www.ensembl.org/). This protocol is as previously described by us (de Bakker et al. 2021). In brief, we isolated total RNA from an embryo using Trizol (Invitrogen) and carried out reverse transcription using SuperScript III (Invitrogen). PCR was performed on these templates using specific primers (Table S2), and the PCR products were cloned in the TOPOTA-PCRII vector (Invitrogen). The inserted amplicons were checked by a PCR with M13-pUC primers located on the TOPOTA-PCRII plasmid and checked on an agarose gel. When they were of the right size they were sent for Sanger sequencing. After confirming the sequence results by BLAST searching, the positive results were used as templates for making the digoxigenin labelled antisense RNA probes. See Table S2 for accession numbers.

The wholemount protocol is as previously described by us (de Bakker et al. 2021). In brief, embryos were fixed in 2 % buffered depolymerised paraformaldehyde (pPFA) for 24 h at 4 °C. They were then washed 3 × with cold PBS and dehydrated through a graded methanol series (25 %, 50 %, 75 % and 100 %) and store at −20 °C. Embryos were rehydrated through a graded methanol series, lightly digested with proteinase K (10 mg/ml in PBS) for 5 min and postfixed in 4 % formaldehyde in PBS after several washes in PBST (PBS pH 7.2 with 0.1 % Tween-20). This was followed by a prehybridization step at 60 °C for at least 3 h or until the embryo had sunk. The hybridization mixture consisted of: 50 % formamide, 2 % Boehringer blocking powder, 5 × SSC (from 20 × standard sodium citrate buffer, 3 M sodium chloride, 0.3 M sodium citrate, pH 7), 1 mg/ml total RNA, 50 μg/ml heparin, 0.1 % Triton X-100, 0.1 % CHAPS (3-[(3-cholamidopropyl) dimethylammonio]-1- propanesulfonate) and 5 mM EDTA (ethylenediaminetetraacetic acid). After the prehybridization mix was removed, we added 400 ng/ml specific probe to fresh hybridization mixture preheated to 60 °C. The embryos were incubated in this mix at 60 °C overnight with slow shaking. The next day the specific probe mixture was removed, collected and stored at −20 °C for reuse. Several stringent washes were done at 60° C to remove non-specifically bound probe [2 × SSC, 0.1 % CHAPS, 50 % formamide]; [2 × SSC 0.1 % CHAPS]; [0.2 × SSC, 0.1 % CHAPS]. After washing several times at room temperature with TBST (0.1 M tris [tris (hydroxymethyl)aminomethane] buffered saline, pH 7.5, 0.1 % Tween-20) the embryos were preincubated with heat inactivated 10 % sheep serum in TBST for 90 min at room temperature followed by overnight incubation with sheep anti-digoxigenin conjugated to alkaline phosphatase (Roche; 1:5,000 dilution in 10 % sheep serum in TBST at 4 °C overnight).

The next day, the non-specifically bound antibodies were washed away by several washes with TBST of which the last one was overnight at 4 °C. The embryos were brought to a higher pH by washing 3 × 10 min in NTT buffer (0.1 M sodium chloride, 0.1 M Tris/HCl, 0.1 % Tween-20, pH 9.5). The enzyme reaction of alkaline phosphate with BM purple (Roche) as substrate results in a blue precipitate. The development of the stain was checked regularly and stopped by washing several times in TBST, removing the substrate and chromogens, and lowering the pH.

2.12. Immunochemistry

Chicken embryos (3 dpe) were fixed and dehydrated as described above in Section 2.11 under 'Wholemount *in situ* hybridization'. They were then processed for paraffin histology using standard protocols (Bancroft and Gamble, 2008). Immunochemistry was performed on 7 μm sections mounted on silane-coated slides (VWR International B.V, Amsterdam). Slides were rehydrated through 2 × xylene, a graded ethanol series (100 %, 90 %, 80 %, 70 %), and demi-water. Slides were then transferred to a container with 0.01 M citric buffer and heated in a microwave to 97 °C. When the slides cooled to room temperature, they were rinsed in PBST. The antibody mix was anti-AP-2α (3B5; Santa Cruz Biotechnology; California, USA; cat. number sc-12726, dilution 1:200) diluted in 1 % bovine serum albumen (BSA) in PBST and added to the slides simultaneously. The slides were returned to the chamber and incubated overnight. After rinsing with PBST, the slides were stained with DAPI (1:1000) for 5 min. Finally, they were washed with PBST 3 × and mounted with ProLong Gold antifade reagent (Invitrogen, USA). The slides were scanned using a Zeiss Axio Scan.Z1. High magnification views were made using a Nikon AX confocal microscope.

2.13. Wholemount TUNEL staining

This protocol is as previously described by us (de Bakker et al. 2021). In brief, embryos were collected and fixed as for *in situ* hybridization rehydrated through a graded methanol series, washed in TBST (0.1 M tris-buffered saline containing 0.1 % Tween), pre-treated with proteinase K (10 mg/ml, 5 min at room temperature), washed in TBST, post-fixed with 4 % formaldehyde in PBST, washed in TBST followed by awash in the TdT buffer (30 mMTris/HCl, 140 mM Na-cacodylate, 0.1 % Triton pH 7.2), preincubated in the reaction mix (70 nM digoxigenin-labeled dUTP, 400 nM ATP, and 1 U/ml terminal transferase in the enzyme buffer) at 4 °C without the cofactor CoCl2 which was added to the reaction mix (1 mM end-concentration) after 1 h. With CoCl2 added, the embryos were incubated at room temperature overnight. The reaction was stopped by adding 200 mM EDTA (ethylenediaminetetraacetic acid), pH 7.0, 1/ 10 of the reaction volume. The digoxygenin-labelled nucleotides were localized with a standard anti-digoxigenin antibody conjugated to alkaline phosphatase procedure followed by staining with BM-purple.

2.14. Vibratome sections

Embryos processed for wholemount *in situ* hybridization, TUNEL, and *in vivo* injection were stored in 1 % pFA in PBS. They were soaked in a mixture of 30 % BSA, 20 % sucrose and 1 % bovine serum gelatine in PBS. The embryos were then placed in 3 ml of fresh mixture in plastic embedding moulds and 240 μL of 10 % glutaraldehyde was added as a hardener. The solidified cubes were trimmed and sectioned at 70 μm in Milli-Q® water and mounted on glass slides with 99.5 % glycerol. The sections from in vivo injection were trimmed and sectioned at 100 μm in Milli-Q® water stained with (i) DAPI; or (ii) DAPI and FM™ 5–95 (N-(3-trimethylammoniumpropyl)-4-(6-(4-(diethylamino)phenyl)hexatrienyl)pyridinium dibromide) supplied by ThermoFisher Scientific. Finally, sections were mounted on glass slides with 99.5 % glycerol.

2.15. Transmission electron microscopy

Primary trunk neural crest cultures as described above in Section 2.9 under 'Localisation of fluorescent 25 nm PS-NPs *in ovo* and *in vitro*'. They were cultured on the Thermanox coverslips (24 mm ⌀; Thermo Fisher Scientific™) pre-coated with rat-tail collagen type-I in *μ-Dish* 35 mm high glass-bottom dishes. The cultures were exposed to 0.1 mg/ml plain PS-NPs 25 nm (1 ml) for 1 h. Coverslips were carefully transferred to 6-well plates and fixed with 2 % glutaraldehyde and 2 % formaldehyde in sodium cacodylate buffer (0.1 M, pH 7.2) for 2 h. Samples were then

incubated with 1 % osmium tetroxide with potassium ferrocyanide (0.8 %) for 1 h. After rinsing, they were stained *en bloc* with 1 % uranyl acetate. The samples were dehydrated through a graded ethanol series (70 %, 90 %, 100 %, 1 h each). Finally, they were embedded in Agar 100 resin kit (cat. number R1031, Agar Scientific, Essex, UK) using propylene oxide as the intermediate reagent, and sectioned at 70 nm on a diamond knife. The sections were examined using a JEOL 1400 + electron microscope.

2.16. Statistical analysis

The statistical analysis was performed in RStudio© (version 1.1.456; https://rstudio.com/. See File S2, File S3). Chi-squared tests and Welch's *t*-tests were used to assess the significance. The correlation of parameters between control and experimental groups were judged by the *P*-value, with significance of ****, $P < 0.0001$; ***, $P < 0.001$; **$P < 0.01$; *$P < 0.05$, ns, $P > 0.05$).

3. Results

3.1. Nanoplastic particles are distributed to multiple organ systems in the embryonic circulation

Characterisation of the nanoparticles used is described in Fig. 1a-d. A preliminary series of experiments on the pharmacokinetics of PS-NPs used fluorescent carboxyl-modified polystyrene particles (500 nm or 1 μm diameter) micro-injected into the embryo. When 500 nm particles were injected into the sub-blastodermal space, some particles crossed the gut and were found in the submucosa, mesentery and mesonephros (Fig. 1e, f) 2 d after. Injection of 1 μm fluorescent particles into the vitelline vein resulted, after 1 d, in distribution of the particles to all vascularised tissues of the body (Fig. 1g, h). The particles particularly accumulated in the liver and the cardiac trabeculae (Movies S1, Movies S2, Movies S3).

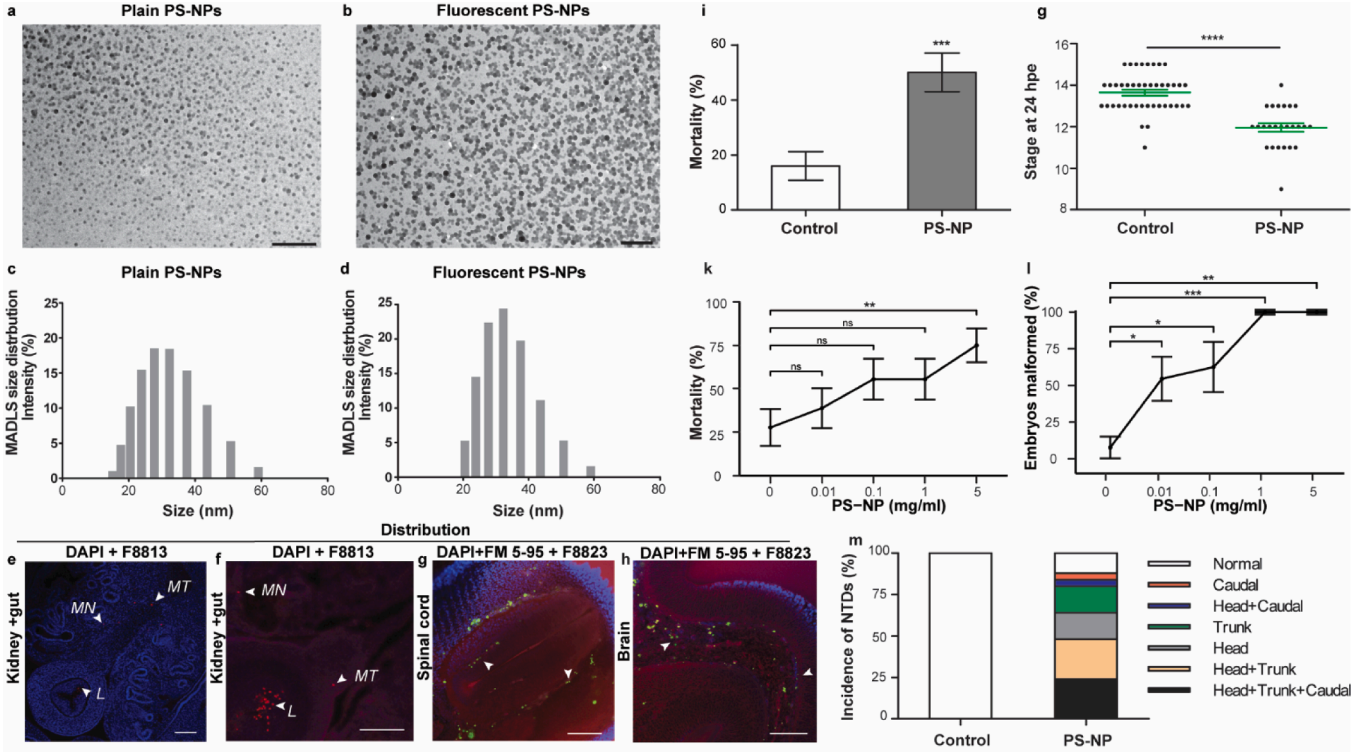

Fig. 1. Physical characterization and biological properties and tissue distribution of PS-NPs. a, b, transmission electron micrographs of 25 nm plain (a) and fluorescent (b) polystyrene nanoplastics in Milli-Q® water. The micrographs show that nanoparticles were spherical in Milli-Q® water. c, d, size distribution of 5 mg/ml 25 nm plain (c) polystyrene and fluorescent (d) nanoplastics in Ringer's solution measured by multi angle dynamic light scattering (MADLS). Both plain and fluorescent polystyrene particles had a nominal diameter of 25 nm. MADLS showed that the plain and fluorescent particles had an actual diameter of 29.32 ± 0.50 nm and 30.62 ± 0.92 nm respectively; and a zeta- (ζ-) potential of −19.54 ± 4.17 mV, and −35.41 ± 1.10 mv respectively in Ringer's solution. e and f, vibratome sections of chick embryos injected at stages 16–17 in the sub-blastodermal cavity with 500 nm ø PS-NPs and examined at 48 hpe in the red fluorescence channel (λ 580/605 nm). Plastic particles appear to have crossed the gut wall (white arrowheads) in two different samples. g and h, vibratome sections of chick embryos injected in the vitelline vein with 1 μm Φ PS-NPs at stages 21–23 and examined at 24 hpe in the green fluorescence channel (λ 505/515 nm). Plastic particles are distributed in vasculature and vascular tissues in an around the spinal cord and brain (white arrowheads). Embryos were exposed at stage 8. i and g, 5 mg/mL PS-NP, analyzed at 24 h post-exposure. i, mortality rate. $n = 50$ (for both control and PS-NPs-treated group) from 5 independent experiments; data are mean ± s.e.m. Chi square test, $P = 0.0007$. G, developmental delay (as expressed in stage; stages according to (Hamburger and Hamilton 1951). $n = 42$ for control and $n = 25$ for PS-NP-treated from 5 independent experiments; data are mean ± s.e.m. Chi square test, $P < 0.0001$. This delay caused by PS-NPs has also been noted by Nie and colleagues Ref. (Nie et al. 2021). k and l, dose–response series, analyzed at 4 d post-exposure. k, mortality. $n = 18$ for 0, 0.01, 0.1 and 1 mg/ml group; $n = 20$ for 5 mg/ml group from 3 independent experiments; data are mean ± s.e.m. Chi square test, $P = 0.7237$ (0 mg/ml vs 0.01 mg/ml), $P = 0.1763$ (0 mg/ml vs 0.1 mg/ml), $P = 0.1763$ (0 mg/ml vs 1 mg/ml), $P = 0.0097$ (0 mg/ml vs 5 mg/ml PS-NPs-treated). l, malformation rate (all malformations). $n = 13$ (0 mg/ml), $n = 11$ (0.01 mg/ml), $n = 8$ (0.1 mg/ml), $n = 8$ (1 mg/ml), and $n = 5$ (5 mg/ml) from 3 independent experiments; data are mean ± s.e.m. Chi square test, $P = 0.0387$ (0 mg/ml vs 0.01 mg/ml), $P = 0.0276$ (0 mg/ml vs 0.1 mg/ml), $P = 0.0002$ (0 mg/ml vs 1 mg/ml), and $P = 0.0016$ (0 mg/ml vs 5 mg/ml). M, axial level affected by neural tube defects (per embryo), 5 mg/mL PS-NP concentration 24 h post-exposure. $n = 42$ for control and $n = 25$ for PS-NP-treated from 5 independent experiments. Key: NTDs, neural tube defects; hpe, hours post-exposure; PS-NP, polystyrene nanoparticles; *L*, lumen of gut; *MN*, mesonephros; *MT*, mesentery; significance of difference between control and experimental groups indicated by asterisks as follows: ****, $P < 0.0001$; ***, $P < 0.001$; **$P < 0.01$; *$P < 0.05$; ns for $P > 0.05$. Scale bars are 200 nm in a and b, and 100 μm in (e-h). (For interpretation of the references to colour in this figure legend, the reader is referred to the web version of this article.)

3.2. Nanoplastics cause developmental delay, increased mortality and are teratogenic

Plain PS-NPs were used in all experiments, except where fluorescent particles were used to track the localisation of PS-NPs. Because particle size may influence the toxicity of NPs (Lee et al. 2019), we made a preliminary series of experiments with 25, 100 and 500 nm plain PS-NPs (File S2). Chicken embryos were exposed at Hamburger-Hamilton (Hamburger and Hamilton 1951) stage 8 (in this and all subsequent experiments), and examined at 4 days post-exposure (dpe). We found that 25 nm PS-NPs produced the highest percentage of malformed embryos, and the highest mortality. Because we kept a fixed concentration (5 mg/mL), our experiments could not disentangle the effects of particle size and particle number. Therefore, the higher mortality and malformation rates at the smaller particle size (25 nm) might be due, in part, to the correspondingly higher number of particles. Nevertheless, we decided to use 25 nm PS-NPs in all subsequent experiments, to limit the number of variables (File S2).

Next, we recorded the mortality and malformations in embryos exposed to 25 nm PS-NPs examined at 24 h post-exposure. The mortality in the treated group (Fig. 1i, File S3) was 50.00 ± 7.07 % which was significantly higher ($P < 0.001$) than in the control group. A significant developmental delay was seen in the surviving, treated embryos (Fig. 1g). The average stage reached was Hamburger-Hamilton stage 11.92 ± 0.21 for treated embryos, and 13.64 ± 0.14 for control embryos (Fig. 1g). In another series, we found that 25 nm PS-NPs produced dose-dependent mortality in embryos exposed at stage 8 and examined at 4 dpe. The highest concentration group (5 mg/ml) had significantly

Fig. 2. Neural tube defects caused by exposure of chick embryos to 25 nm PS-NPs. a-j, micro-CT images of control (a-e) and 25 nm PS-NPs treated embryos (f-j). $n = 2$ for both groups. a, stage 14, volume rendering of wholemount control chick embryo. (b-e), virtual transverse sections. f, stage 12, volume rendering of wholemount PS-NPs treated embryos. (g-j), virtual transverse sections. White arrowheads in f-j indicate neural tube abnormalities. (k-u), wholemount and histological sections of control (k-n) and 25 nm PS-NPs treated embryos (o-u). k, stage 13, control embryo. (l-n), transverse sections, haematoxylin and eosin stain. o, stage 12, PS-NP-treated embryo. (p-u), transverse sections, haematoxylin and eosin stain; black arrowheads, neural tube abnormalities; black arrows, clumps of detached neural crest cells (as shown by gene expression in Fig. 5). Scale bars, 500 μm in (a, f, k, o), 200 μm in (b-e, g-j, l-n, p-u). *Key*: In figures a, f, k and o, the dashed horizontal lines indicate the plane of the associated transverse sections. PS-NP, polystyrene nanoparticles. *Note.* the embryos in f and o both have neural tube defects

higher mortality (75.00 ± 9.68 %; $P < 0.01$), compared to the control group (Fig. 1k, File S3).

3.3. Nanoplastics cause malformations in multiple organ systems

Exposure to PS-NPs led to a far wider spectrum of malformations than has previously been reported (Nie et al. 2021). Furthermore, we find that the malformations are produced by PS-NPs in a dose-dependent manner which is statistically significant (Fig. 1l). Exposure to 5 mg/ml led to malformations in 100 % of survivors (Fig. 1l, File S3).

Half of the embryos ($n = 16/32$) showed a failure of the normal processes of flexure (dorsoventral bending of the primary axis), and/or torsion (rotation along the primary axis). These failures lead to the embryo being abnormally flat, or straight, or both (Fig. S1d, e, f, k, l therein). The tailbud was hypoplastic or absent in 5/32 embryos at 4 dpe (Fig. S1n). In some embryos the caudal neural tube showed gross dysplasia, presenting as an asymmetric mass of disorganized tissue (Fig. S1, bottom). In other embryos, the cranial neural plate was open and abnormally thickened (Fig. S1k). Microphthalmia was present in 8/32 embryos in the form of gross hypoplasia or dysplasia of the optic cup and lens (Fig. S1c, i, n, File S4). The microphthalmia was unilateral in 3 embryos and bilateral in 5.

All further *in ovo* experiments in this study used a single concentration of PS-NPs (5 mg/ml), with Ringer's only as the vehicle-only control. In embryos fixed at 24 h post-exposure (hpe; Fig. 1i, g) we found 25 survivors out of 50 treated embryos, and 22 of the survivors showed neural tube defects (failure of the neural tube to close dorsally (Copp et al. 2013); Fig. 2, Movies S4, Movies S5, Movies S6). While neural tube defects were seen at all axial levels along the neural tube, no defects were observed in control embryos (Fig. 1m).

In treated embryos analysed at 8 dpe, 2/6 had craniofacial dysplasia, 2/6 had cleft primary palate, 1/6 had both, and 1/6 had no craniofacial malformations (Fig. S2, File S4). The embryos with craniofacial dysplasia lacked the palatine, maxillary and premaxillary cartilages. In three cases, Meckel's cartilage was present, but not fused in the midline. There were no craniofacial malformations in the controls ($n = 6$). Embryos with neural tube defects showed concomitant vertebral defects (spina bifida; Fig. S2).

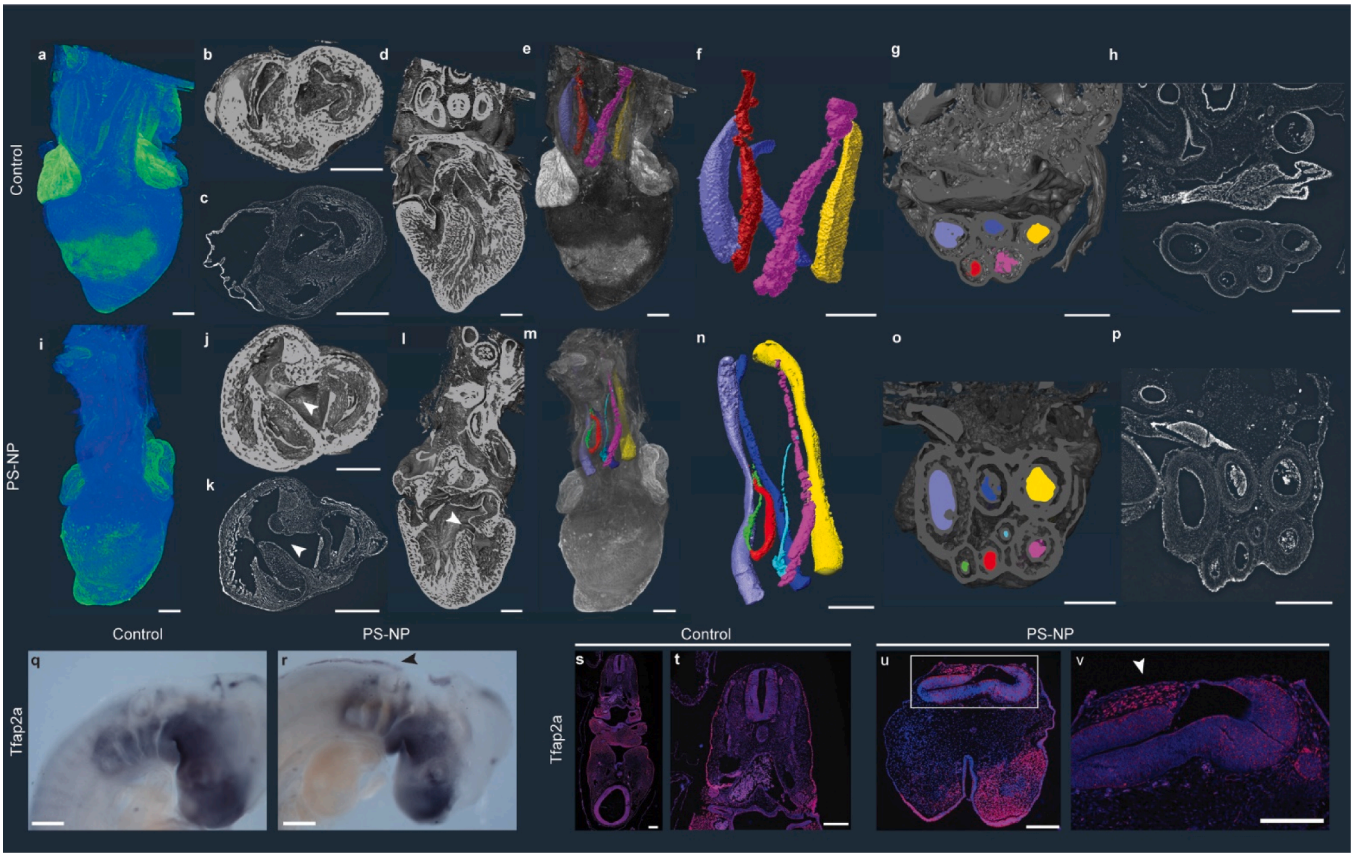

Fig. 3. 25 nm PS-NPs cause cardiac malformations by disrupting the development of the cardiac neural crest. a-p, synchrotron tomographic scans of hearts and great vessels at 8 dpe; a-h, control embryo, stage 35. $n = 2$. a and e, segmentation and volume rendering of heart and vessels. (b, d, g), virtual transverse sections. (c, h) two-dimensional (2-D) view of virtual transverse sections. (f), three-dimensional (3-D) model of great vessels produced by manual tracing. (i-p), PS-NP treated, stage 35. $n = 2$. (i, m), volume rendering of PS-NPs treated heart. (n), 3-D model of great vessels produced by manual tracing. (j, n, o), 3-D view of virtual transverse sections. (k, p), 2-D view of virtual transverse sections. (q, r), wholemount *in situ* hybridization of TFAP2A. (q), control embryo, stage 19. $n = 2$. (r), PS-NPs treated embryo, stage 18. $n = 3$. s-v, immunohistochemistry showing TFAP2A and DAPI stained transverse sections. $n = 2$ for control and $n = 5$ for PS-NPs-treated group. (s, t), control chicken embryo, stage 19. (u, v), PS-NPs treated chicken embryo, stage 17. *Note*, The treated heart in (i-p) has both a ventricular septal defect (arrowhead) and supernumerary pharyngeal arch arteries (seven in place of the normal five). The two supernumerary pharyngeal arch arteries (green and light blue) are aberrant subclavian arteries. In this embryo, the brachiocephalic artery is abnormally short. The sixth pharyngeal arch arteries are normal in all of our specimens from control group. The wholemount *in situ* hybridization for the cardiac neural crest marker TFAP2A shows that PS-NP treatment causes a failure of the cardiac neural crest to completely populate the pharyngeal arches; it also disrupts migration of the cardiac neural crest, such that some crest cells never leave the neural tube (arrows). Key: purple, right aorta; red, right brachiocephalic artery; yellow, left pulmonary artery; pink; left brachiocephalic artery; blue, right pulmonary artery; green right subclavian artery; light blue, left subclavian artery; PS-NP, embryos treated with polystyrene nanoparticles (25 nm, 5 mg/mL); dpe, days post-exposure. Scale bars, 500 μm in (a-p), 300 μm in (q, r), 200 μm in (s, v). (For interpretation of the references to colour in this figure legend, the reader is referred to the web version of this article.)

3.4. Heart malformations and abnormal circulatory function in nanoplastic-treated embryos

When we examined living embryos *in ovo*, we found that PS-NP treated embryos showed a significant decrease in heart rate (bradycardi) at 3 dpe (Fig. S3a, b, Movies S7, Movies S8, Movies S9, Movies S10). There was no significant effect on heart rate in embryos at 2 dpe. Another abnormality we noted in PS-NPs treated embryos was an abnormal widening of vitelline blood vessels (Fig. S3c, d). In some of the PS-NP treated embryos, the two dorsal aortae fuse ectopically. PS-NP treated embryos also show signs of cardiac defects when examined alive, *in ovo*, at 2 and 3 dpe. There was an abnormal abundance of cardiac jelly which continued into the apex of the heart in treated embryos. Furthermore, the cardiac jelly appeared to be less cellular, most likely because of a diminished endothelial-mesenchymal transition in the endocardium; Fig. S3e-m). The myocardium also showed signs of being abnormally thin in the treated embryos (Fig. S3n-p). We could not quantify any of these features in the beating hearts.

Synchrotron tomographic scanning and histology at 8 dpe showed malformations of the heart and great arteries (Fig. S4) in treated embryos. Of seven treated embryos, three had a ventricular septal defect (Fig. 3j-l), two had persistent or extra pharyngeal arch arteries (Fig. 3m-p), one had persistent truncus arteriosus and two had aortopulmonary septal defects (Fig. S4, File S4). Expression analysis of the neural crest marker gene TFAP2A shows that the migration of crest cells into the pharyngeal arches is disrupted in the PS-NP treated embryos, with some neural crest cells remaining behind in the dorsal midline (Fig. 3q-v).

3.5. Nanoplastics selectively localize to neural crest cells

To track the distribution of PS-NPs, stage 8 chicken embryos were exposed *in ovo* to 50 μL fluorescein-labelled 25 nm PS-NPs for 2, 6 and 24 h. Confocal microscopy showed that fluorescence was subsequently localised to cell masses in the dorsal midline of the neural tube (Fig. 4a-d) This corresponds to the region where neural crest cells develop. Labelled cell masses were also seen protruding into the lumen from the dorsal aspect of the neural tube, or lying free in the lumen. We found that primary cultures of neural crest cells showed an uptake of fluorescent PS-NPs within 2–6 h (Fig. 4e). Transmission electron microscopy of the cultured cells showed inclusions or lacunae that were consistent with

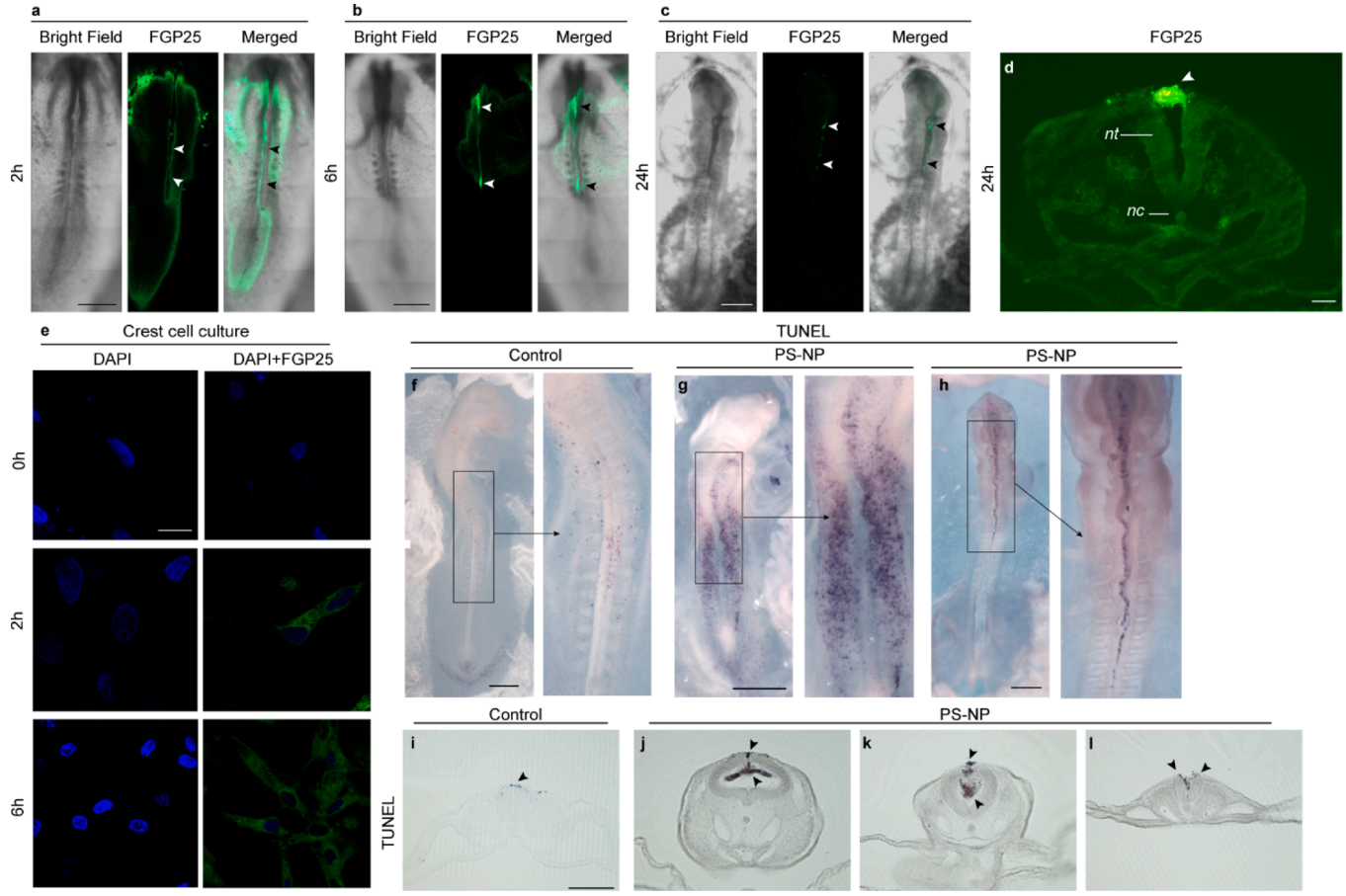

Fig. 4. Tissue distribution, selective localization, and induction of cell death in neural crest cells, by PS-NPs. a-c, chick embryos exposed to fluorescent PS-NPs (FGP, green florescence) examined at 2, 6 and 24 h, respectively. $n = 2$ for all different time series. a, 2 hpe PS-NPs treated chick embryos, stage 8. b, 6 hpe PS-NPs treated chick embryos, stage 9. c, 24 hpe PS-NPs treated chick embryos, stage 13. In a-c, there is strong fluorescence (green) associated with the dorsal midline of the neural tube (note that the chicken embryos did not show autofluorescence). d, transverse cryosection (25 μm). There is strong fluorescence (green) in a cellular mass lying in between the neural folds (white arrow). e, neural crest cells stain with DAPI (blue florescence) exposed *in vitro* to fluorescent PS-NPs (green florescence) and examined at 0, 2, and 6 h, respectively. TUNEL staining of control (j) and PS-NP-treated (g and h) chick embryos. $n = 2$ for control and $n = 3$ for PS-NP treated group. (f), stage 14, (g), stage 12, (h), stage 12 (N.B. all embryos are 2 d incubation, but g and h show a developmental delay caused by PS-NP treatment). In g and h, note the extensive cell death, and dead cells in the dorsal midline. i-l, TUNEL staining on vibratome sections. $n = 2$ for both control and PS-NPs-treated chick embryos. i, control, stage 14. j-l, PS-NPs-treated, stage 12. PS-NPs treatment resulted in clumps of dead cells in the neural folds and in the neural tube lumen (black arrowhead). *Key*: hpe: hours post-exposure, PS-NP, embryos treated with polystyrene nanoparticles, 25 nm, 5 mg/mL. *nt*: neural tube, *nc*: notochord. Scale bars, 500 μm in (a-c, f-h), 200 μm in (i-l), 50 μm in (d), 20 μm in (e). (For interpretation of the references to colour in this figure legend, the reader is referred to the web version of this article.)

PS-NPs in the cytoplasm (Fig. S5).

To confirm the neural crest identity of the affected cells, we studied the expression of a panel of neural crest markers (Martik and Bronner 2021), namely: WNT1, FOXD3, SNAI2 (SLUG, SNAIL2), LMO4, SOX10, PAX3 and TFAP2A (Table S2). We found that PS-NP treated embryos showed that the cells remaining in the dorsal midline, or the margins of the open neural tube, express neural crest markers (Fig. 5). These findings were consistent across all seven neural crest markers (Fig. 5q, r). PS-NPs treatment also triggered a wave of cell death in the putative neural crest cells (Fig. 4h, j-l).

4. Discussion

We have described a wide spectrum of severe malformations in chicken embryos exposed *in ovo* to 25 nm PS-NPs. The malformations include neural tube and craniofacial defects, as noted previously (Nie et al. 2021). In addition, we observed microphthalmia, heart malformations, bradycardia, persistent or extra pharyngeal arch arteries, maxillary hypoplasia, axial defects, tail aplasia and, in one specimen, bilateral phocomelia of the hindlimbs. We also found that treated embryos showed defective cellularization of the cardiac jelly, abnormal blood vessels, thinned myocardium. This is a much wider spectrum of malformations than previously reported, and we report congenital heart defects for the first time. Furthermore, we have identified neural crest cells disruption as the major mechanism of PS-NPs toxicity. This mechanism (Fig. 6) can account for most or all of the malformations we observed.

We find neural tube defects in the head, trunk, tail, or a combination of these sites. This variation in location could be because of differences in distribution of PS-NPs between treated embryos; or could be a result of multiple neural tube closure sites in one embryo (as has been postulated for human malformations (Seller 1995). Neural tube defects are known to result from a failure of the neural folds to meet and close (Copp and Greene 2013; Copp et al. 2013). We suggest this failure of fusion is due to toxic effects of PS-NPs on the neural crest — a population of neuroectodermal cells adjacent to the fusion zone of the closing neural tube (Creuzet 2009; Green et al. 2015; Le Douarin et al. 2012; Le Douarin and Kalcheim 1999; Martik and Bronner 2021; Waldo et al.

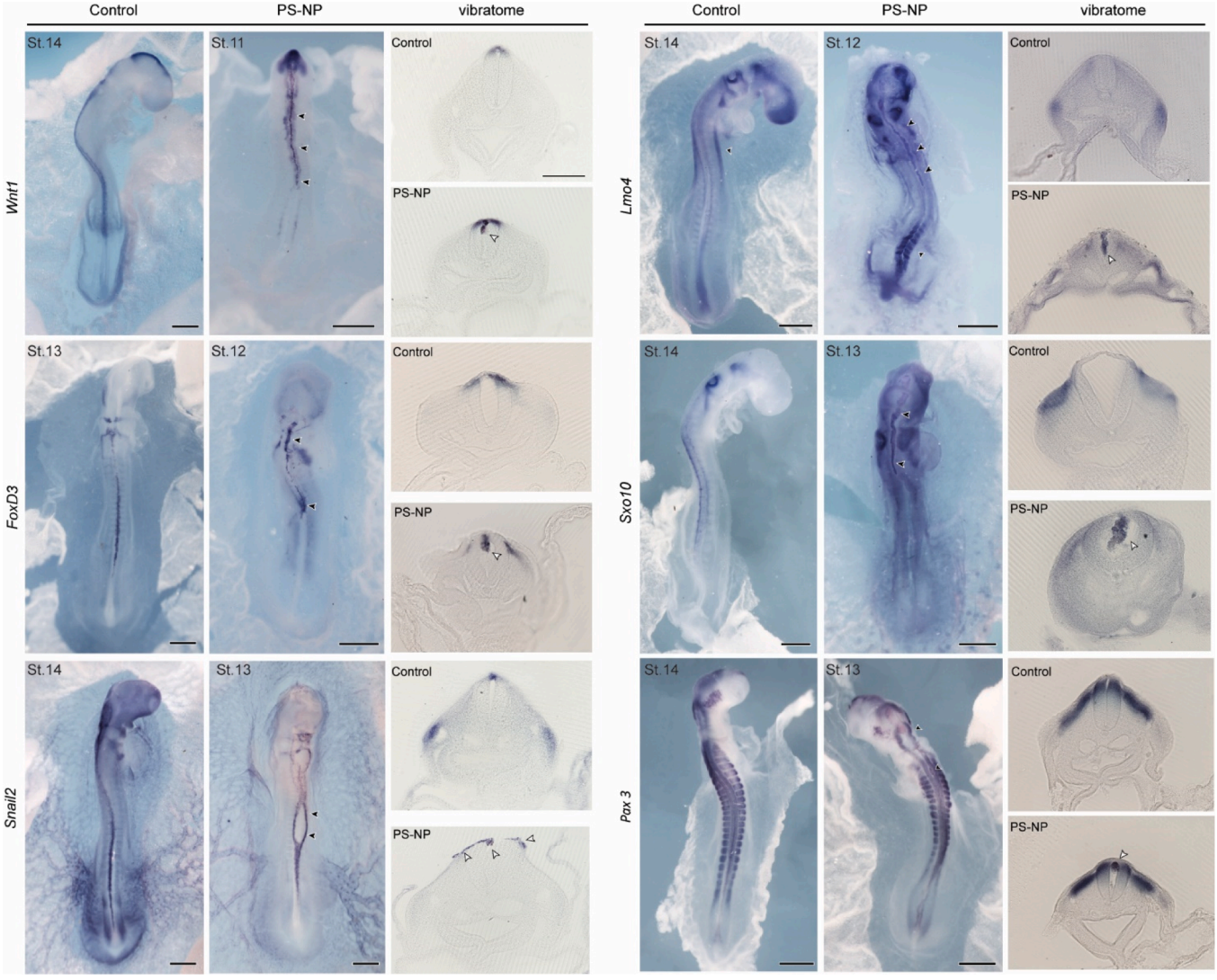

Fig. 5. Cells disrupted by 25 nm PS-NPs express neural crest markers. All embryos were exposed at stage 8 to 50 μL plain PS-NPs (5 mg/mL). $n = 3$ for both control and PS-NP treated group of all genes. Note, all embryos are two days incubation; the treated embryos all showed developmental delay relative to the controls. Cellular debris of neural crest cells (arrowheads). *Key*: PS-NP, embryos treated with polystyrene nanoparticles, 25 nm, 5 mg/mL. Arrowheads in the treated embryos indicate putative neural crest cells. In WNT1 and FOXD3 *in situs*, the cells are clumped. In SNAI2 *in situs*, there are putative neural crest cells at the margins of the neural tube defect. In all cases except the SNAI2 *in situ* shown, there are putative neural crest cell clumps inside the neural tube lumen. Scale bars, 500 μm in wholemount embryos, 200 μm in vibratome transverse sections.

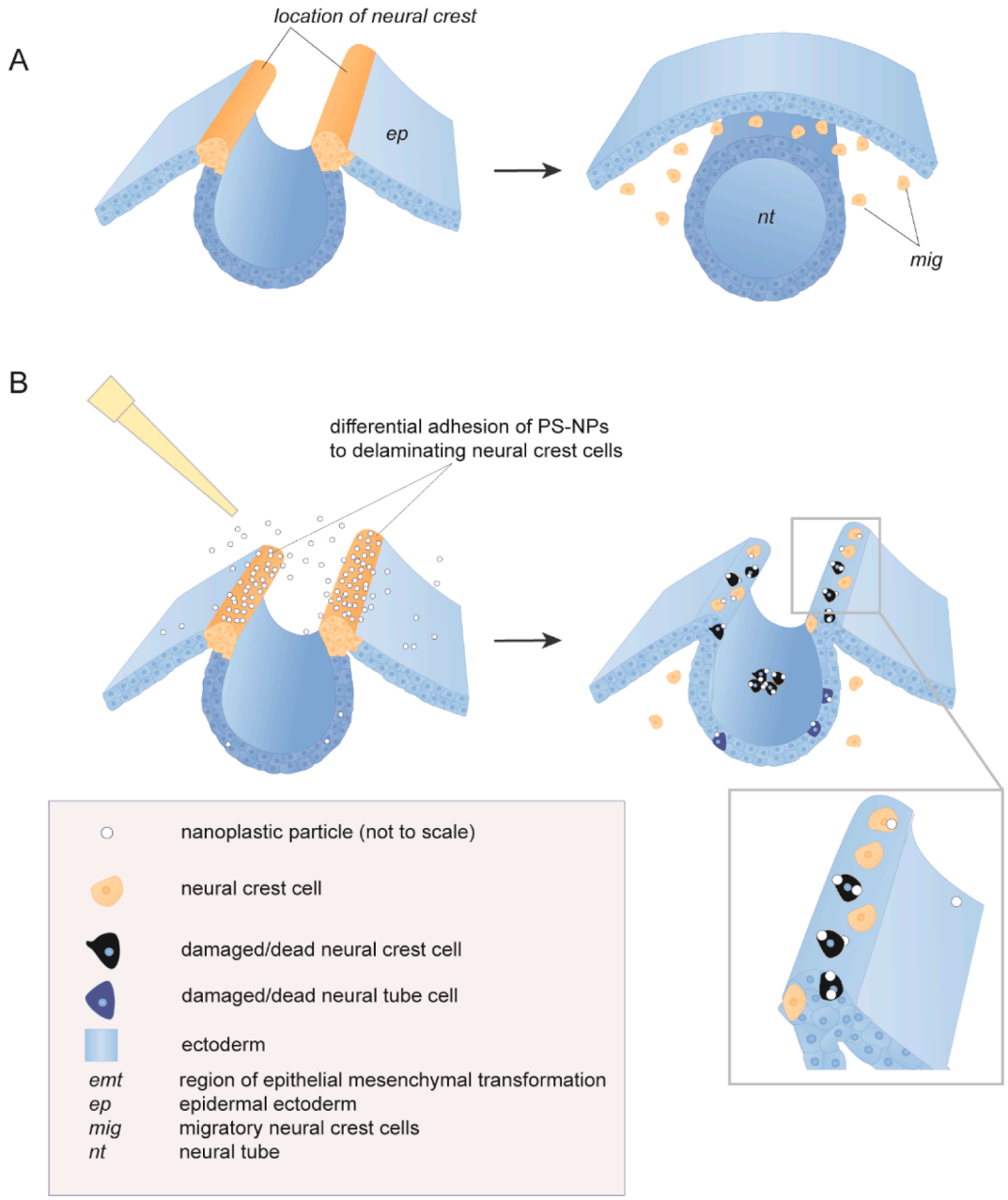

Fig. 6. Our hypothesis of PS-NP-induced developmental toxicity, based on disruption of neural crest development. A, normal development of the neural tube and neural crest. B, development of the neural tube and crest after exposure of the embryo to 25 nm PS-NPs. We hypothesize that the nanoparticles adhere selectively to the neural crest cells undergoing epithelial-mesenchymal transition, and induce cell death in at least a subpopulation of those neural crest cells. This reduces the number of normal neural crest cells, disrupts their migration and interferes with the normal closure of the neural tube. It also often leaves a clump of putative neural crest cells in the lumen of the neural tube (or the neural groove, in the case of a neural tube defect). We suggest that these events lead to neural tube defects, microphthalmia, craniofacial and cardiac malformations. Note that we saw some evidence of very limited cell death in the neural tube induced by PS-NPs (as shown in this figure).

1998). This model is consistent with a study showing that the neural crest is essential for neural tube closure, at least in the cranial region (Creuzet 2009; Creuzet et al. 2006).

We have provided here the first evidence that PS-NP exposure can cause heart malformations. It has previously been shown that such malformations can also be produced in the chicken embryo by surgical ablation of the cardiac neural crest (Keyte and Hutson 2012; Kirby and Waldo 1995), that is, the crest cells at the axial level between the otocyst and somite three (Hutson and Kirby 2007). The early-stage cardiovascular abnormalities that we observed have also been reported in other studies in which pre-migratory cardiac neural crest were surgically ablated (Waldo et al. 1999). At later stages, treated embryos showed instances of abnormal branching of the pharyngeal arch arteries, ventricular septal defects and aortopulmonary septal defects. These malformations likely arise because of damage to the neural crest, which is essential for normal development of the aortopulmonary septal complex of the heart and the wall of the great vessels (Bradshaw et al. 2009; Erhardt et al. 2021; Hutson and Kirby 2007; Kirby and Waldo 1995; Newbern et al. 2008; Poelmann et al. 1998; Porras and Brown 2008; Snarr et al. 2008). We also observed epicardial blebbing, probably caused by disturbed fluid handling of the developing coronary system that showed scant arterial development and no ingrowth into the neural crest-dependent aortic root (Gittenberger-de Groot et al. 2012). We also noted ectopia cordis, a phenotype associated with congenital cardiac

malformations in human such as double outlet right ventricle (Malik et al. 2015).

In addition to cardiac malformations, we often saw hypoplasia or aplasia of the upper beak, and failure of Meckel's cartilage to fuse with its contralateral partner. The co-occurrence of cardiac and craniofacial malformations in our study is consistent with the fact that the cranial neural crest contributes to the development of both the heart and the facial skeleton (Keyte and Hutson 2012). The idea of a mechanistic link between cardiac and craniofacial development is embodied in the concept of the 'cardiocraniofacial module' (Keyte and Hutson 2012). Furthermore an association of cardiac and craniofacial malformations is seen in clinical syndromes such as DiGeorge syndrome (chromosome 22q11.2 deletion syndrome) (Escot et al. 2016; McDonald-McGinn and Sullivan, 2011).

Interestingly, it was previously shown that the exposure of chicken embryos to metal nanoparticles (zinc oxide) causes craniofacial abnormalities, which was they suggested to result from disruption of neural crest development (Yan et al. 2020). However, many types of metal nanoparticles shed ions, and so the toxicity observed in that study may not be mediated by the same mechanisms as nanoplastics. It should also be noted that craniofacial defects that we observed here are not necessarily a reflection of abnormal neural crest development. Craniofacial defects are sometimes associated with neural tube defects in the head region; this association, whether causal or not, has been described in terms of the 'brain–cranium–face triad' (Gondré-Lewis et al. 2015).

The occurrence in our experiments of microphthalmia (where one or both eyes is abnormally small;Verma and Fitzpatrick 2007) might also be explained by the fact that neural crest cells are important for the normal development and growth of the eye (Bryan et al. 2020; Grocott et al. 2011). This is supported by a study in which surgical ablation of the cranial neural crest in the chick embryo can lead to microphthalmia (Creuzet 2009). The gene TFAP2A (Brewer et al. 2002) is a neural crest marker gene. Interestingly, mutations in this gene in humans can lead to facial malformations and microphthalmia, as well as other eye defects (Gestri et al. 2009). Other studies show a functional link between the neural crest and normal eye development (Weigele and Bohnsack, 2020).

Our experiments with fluorescent PS-NPs show strong labelling in the neural crest, but little or none in any other tissues. Furthermore, we find that that fluorescence is seen in the cytoplasm within 2 h and is still there at 6 h. However, these experiments should be interpreted with caution because: (i) single 25 nm particles are too small to be directly visualised with optical microscopes; and (ii) it is possible that the fluorescence we saw was partly due to leakage of the fluorochrome from the particles. In any case, it is evident that strong fluorescence is specifically found in neural crest cells.

Our TUNEL-labelling experiments showed enhanced cell death in both the dorsal midline of the neural tube, and in ectopic clumps of cells in the neural tube lumen that we identified as neural crest cells with neural crest markers. The same markers also identify a population of neural crest cells in the dorsal midline of PS-NP treated embryos that have failed to migrate. We also see evidence of reduced neural crest cell migration into the pharyngeal arches. Together, these data suggest that neural crest cells are damaged, or undergo cell death after binding PS-NPs, and fail to migrate. Candidate mechanisms of PS-NPs cell-damage include the denaturation of proteins (Gopinath et al. 2019; Hollóczki and Gehrke 2019), and the accumulation of PS-NPs in the cytoplasm, after being taken up by endocytosis, and then resisting degradation by lysosomal enzymes (Nie et al. 2021). Our hypothesis, that PS-NPs inhibit neural crest migration, is consistent with experiments on other migratory cell types. For example, it has been shown that PS-NPs supress the migration and dispersion of aggregated CT26 murine carcinoma cells *in vitro* (Beaune et al. 2019).

In a few treated embryos, the tailbud was hypoplastic or aplastic; one embryo showed agenesis of the tail and phocomelia of the hindlimbs. We suggest that these effects reflect an effect of PS-NPs on surface-exposed mesenchymal populations in the primitive streak of the tailbud. During gastrulation, and the process of ingression, the dorsal surface epithelium undergoes an epithelial-mesenchymal transition with local loss of the basal lamina (Bellairs 1986; Shook and Keller 2003). This process is still active at the stage when we introduced the PS-NPs to the egg (Knezevic et al. 1998).

Another potential source of mesenchymal cells in the caudal region, that might be affected by PS-NP exposure, is the junction between regions of primary and secondary neurulation (Dady et al. 2014). This process starts around stage 8 (Dady et al. 2014). Binding of the PS-NPs to these junctional mesenchymal cells could explain the gross dysplasia of the neural tube in the caudal region of some embryos. We exposed embryos to PS-NPs at stage 8; both gastrulation and neurulation are still active at this stage (Keibel and Abraham 1900).

Our data show that 25 nm PS-NPs selectively attach to neural crest cells, and possibly other cell populations undergoing epithelial-mesenchymal transformation on the dorsal surface of the embryo. By contrast, PS-NPs show little or no attachment to intact embryonic epithelia. It is possible that this reflects the differential expression of adhesion molecules on different cell populations on the surface of the embryo. For example, sugar residues in the cell coat of neural crest cells in mouse and rat embryos differ considerably from neurectoderm and epithelial ectoderm (Smits-van Prooije et al. 1986). Furthermore the cell adhesion molecule cadherin 6B is differentially expressed on pre-migratory crest cells and cadherin 7 is expressed on migratory crest cells (Taneyhill and Schiffmacher, 2017). Note that the switch between the expression of different cadherin molecules (the 'cadherin switch') accompanies the segregation of the neural crest lineage from the neurectoderm (Dady et al. 2012). Our hypothesis is that PS-NPs may interact with the cadherins during neurulation, possibly changing the protein structure and functions (Hollóczki and Gehrke 2019). The interaction of proteins with nanoplastics is the basis of the 'corona' which is sometimes observed on nanoparticles exposed to proteins (Kihara et al. 2021; Röcker et al. 2009).

The concentration of nanoparticles used in this study (5 mg/mL) is higher than that reported, for example, in human blood. (Leslie et al. 2022). However, it should be remembered that PS-NPs and other nanomedicines are likely to be used in high concentrations. Furthermore, it has been shown that nanoplastics can be transmitted to offspring in several animal models (Pitt et al. 2018; Zhao et al. 2017); if this applies to humans, then we might expect a cumulative increase in particles in human tissues over the generations.

The highly-selective effect of PS-NPs on embryonic neural crest cells may mean that they are capable of disrupting development even in low levels exposures. Furthermore, detecting nanoplastics in the environment and in human tissues, is extremely difficult, and the associated analytics are in their infancy. As a result, it is likely that human exposure to PS-NPs has been substantially underestimated. Finally, it is worth remembering that even if society stops now with all plastic pollution, the weathered nanoplastic debris levels from existing plastics in the environment will still increase. In the future, we will need more information about the teratogenicity of nanoplastics — and possibly of nanomaterials in general.

5. Conclusions

Our study shows that PS-NPs cause effects on development that closely resemble those produced by a surgical ablation of the neural crest (Bockman et al. 1987; Hutson and Kirby 2007; Kirby 1999; Kirby et al. 1989; Kirby et al. 1985). This means that nanoplastics can have catastrophic effects on development by 'targeting' a specific subpopulation of embryonic cells. The targeting is passive, in the sense that PS-NPs may simply show strong binding to certain cell-surface molecules on neural crest cells. In any case, the highly selective effect of PS-NPs on certain exposed embryonic cell populations may mean that they are capable of disrupting development even in low-level exposures. The

production of malformations by NPs are of concern, given the extensive environmental exposure of humans to small plastic particles (Anagnosti et al., 2021; Cox et al., 2019; Koelmans et al., 2019; Vighi et al., 2021; Zhang et al., 2020), the reported presence of small plastic particles in human tissues (Jenner et al. 2022; Leslie et al. 2022; Ragusa et al.), and the current development of a new generations of nanomedicines intended for human therapeutic use (Boehnke et al. 2022). In summary, we believe that PS-NPs of primary or secondary origin pose a potential danger to living embryos of humans and other vertebrates. Because of this, the increasing burden of environmental nanoplastics is a matter for concern.

Author Contributions

M.W. carried out the experiments and wrote the paper; M. Rücklin helped with microCT and synchrotron X-ray tomographic microscopy, and provided funding; R.E.P. analysed the cardiac malformations; C. deM. performed *in situ* hybridisation and immunochemistry; M.F. performed statistical analyses; G.E.M.l. helped with fluorescent imaging and transmission electron microscopy; M.A.G.deB. helped with *in situ* hybridisation and TUNEL staining; E.C. helped analyse cardiac malformations; L.J.B. performed *in situ* hybridisation; F.M. helped with synchrotron X-ray tomographic microscopy; B.J.W. helped with immunohistochemistry; M.C. de R. provided histology and slide-scanning facilities; S.C. performed vitelline vein injections and L.N. performed sub-blastodermal injections; M.V. helped supervise the project, provided expertise on nanoparticles, helped characterise the particles and provided funding; M.K.R. conceived the project, provided supervision, helped write the paper and provided facilities and funding.

Funding Sources

We are grateful for the support of the ERC-C grant (number 101002123) entitled 'EcoWizard'. We thank the Chinese Scholarship Council (CSC) for its financial support to Meiru Wang (scholarship number 201908210335).

Data availability statement

The datasets reported in this paper are available from the corresponding author on reasonable request.

CRediT authorship contribution statement

Meiru Wang: Data curation, Methodology, Investigation, Writing – original draft. **Martin Rücklin:** Software, Supervision, Funding acquisition, Writing – review & editing. **Robert E. Poelmann:** Investigation, Supervision, Writing – review & editing. **Carmen L. de Mooij:** Investigation, Data curation, Writing – review & editing. **Marjolein Fokkema:** Formal analysis, Methodology, Writing – review & editing. **Gerda E.M. Lamers:** Investigation, Visualization, Writing – review & editing. **Merijn A.G. de Bakker:** Investigation, Validation, Writing – review & editing. **Ernest Chin:** Investigation, Writing – review & editing. **Lilla J. Bakos:** Investigation, Writing – review & editing. **Federica Marone:** Visualization, Writing – review & editing. **Bert J. Wisse:** Resources. **Marco C. de Ruiter:** Resources. **Shixiong Cheng:** Investigation. **Luthfi Nurhidayat:** Investigation. **Martina G. Vijver:** Supervision, Conceptualization, Funding acquisition, Writing – review & editing. **Michael K. Richardson:** Conceptualization, Data curation, Writing – original draft, Supervision, Funding acquisition, Writing – review & editing, Project administration.

Declaration of Competing Interest

The authors declare that they have no known competing financial interests or personal relationships that could have appeared to influence the work reported in this paper.

Data availability

Data will be made available on request.

Acknowledgements

We thank Bertie Joan van Heuven of Naturalis for help with microCT scanning. Dr. Fazel Abdolahpur Monikh is thanked for his advice about nanoplastics. Yuchao Song helped with MADLS. Aleksandr Mironov kindly advised on transmission electron microscopy techniques. Dr. Joost Willemse wrote program code to measure the heart rate. We thank the Paul Scherrer Institut, Villigen, Switzerland, for provision of synchrotron radiation beamtime at the TOMCAT (X02DA) beamline of the Swiss Light Source.

Appendix A. Supplementary material

Supplementary data to this article can be found online at https://doi.org/10.1016/j.envint.2023.107865.

References

Anagnosti, L., Varvaresou, A., Pavlou, P., Protopapa, E., Carayanni, V., 2021. Worldwide actions against plastic pollution from microbeads and microplastics in cosmetics focusing on European policies. Has the issue been handled effectively? Marine Pollut. Bull. 162 https://doi.org/10.1016/j.marpolbul.2020.111883.

Auta, H.S., Emenike, C.U., Fauziah, S.H., 2017. Distribution and importance of microplastics in the marine environment: A review of the sources, fate, effects, and potential solutions. Environ. Int. 102, 165–176. https://doi.org/10.1016/j.envint.2017.02.013.

Ball, P., 2021. Cleaning the seas with blue diesel. Nat Mater 20, 1588. https://doi.org/10.1038/s41563-021-01164-3.

Bancroft, J.D., Gamble, M., 2008. Theory and practice of histological techniques. Elsevier health sciences.

Beaune, G., Nagarajan, U., Brochard-Wyart, F., Winnik, F.M., 2019. Polymeric Nanoparticles Limit the Collective Migration of Cellular Aggregates. Langmuir 35, 7396–7404. https://doi.org/10.1021/acs.langmuir.8b01736.

Bellairs, R., 1986. The primitive streak. Anat Embryol (Berl) 174, 1–14. https://doi.org/10.1007/BF00318331.

Bergmann, M., Mützel, S., Primpke, S., Tekman, M.B., Trachsel, J., Gerdts, G., 2019. White and wonderful? Microplastics prevail in snow from the Alps to the Arctic. Science advances 2019; 5: eaax1157.

Bockman, D.E., Redmond, M.E., Waldo, K., Davis, H., Kirby, M.L., 1987. Effect of neural crest ablation on development of the heart and arch arteries in the chick. AmJAnat 180, 332–341. https://doi.org/10.1002/aja.1001800403.

Boehnke, N., Straehla, J.P., Safford, H.C., Kocak, M., Rees, M.G., Ronan, M., Rosenberg, D., Adelmann, C.H., Chivukula, R.R., Nabar, N., Berger, A.G., Lamson, N.G., Cheah, J.H., Li, H., Roth, J.A., Koehler, A.N., Hammond, P.T., 2022. Massively parallel pooled screening reveals genomic determinants of nanoparticle delivery. Science 2022; 377: eabm5551, 10.1126/science.abm5551.

Bradney, L., Wijesekara, H., Palansooriya, K.N., Obadamudalige, N., Bolan, N.S., Ok, Y.S., Rinklebe, J., Kim, K.-H., Kirkham, M.B., 2019. Particulate plastics as a vector for toxic trace-element uptake by aquatic and terrestrial organisms and human health risk. Environ. Int. 131, 104937.

Bradshaw, L., Chaudhry, B., Hildreth, V., Webb, S., Henderson, D.J., 2009. Dual role for neural crest cells during outflow tract septation in the neural crest-deficient mutant Splotch(2H). J Anat 214, 245–257. https://doi.org/10.1111/j.1469-7580.2008.01028.x.

Brady, J., 1965. A simple technique for making very fine, durable dissecting needles by sharpening tungsten wire electrolytically. Bulletin of the Georgian Academy of Sciences. World Health Org. 32, 143.

Brewer, S., Jiang, X., Donaldson, S., Williams, T., Sucov, H.M., 2002. Requirement for AP-2alpha in cardiac outflow tract morphogenesis. Mech Dev 110, 139–149. https://doi.org/10.1016/s0925-4773(01)00579-2.

Brun, N.R., van Hage, P., Hunting, E.R., Haramis, A.G., Vink, S.C., Vijver, M.G., Schaaf, M.J.M., Tudorache, C., 2019. Polystyrene nanoplastics disrupt glucose metabolism and cortisol levels with a possible link to behavioural changes in larval zebrafish. Commun Biol 2, 382. https://doi.org/10.1038/s42003-019-0629-6.

Bryan, C.D., Casey, M.A., Pfeiffer, R.L., Jones, B.W., Kwan, K.M., 2020. Optic cup morphogenesis requires neural crest-mediated basement membrane assembly. Development 2020; 14710.1242/dev.181420.

Butler, K.S., Brinker, C.J., Leong, H.S., 2022. Bridging the In Vitro to In Vivo gap: Using the Chick Embryo Model to Accelerate Nanoparticle Validation and Qualification for In Vivo studies. ACS Nano. https://doi.org/10.1021/acsnano.2c03990.

Chauhan, G.S., Wani, S., 2019. Plastic pollution: A major environmental threat. Int. J. Innovat. Res. Technol. 6, 43–46.

Cohen, A.M., Konigsberg, I.R., 1975. A clonal approach to the problem of neural crest determination. Dev Biol 46, 262–280. https://doi.org/10.1016/0012-1606(75)90104-9.
Copp, A.J., Greene, N.D., 2013. Neural tube defects–disorders of neurulation and related embryonic processes. Wiley Interdiscip Rev Dev Biol 2, 213–227. https://doi.org/10.1002/wdev.71.
Copp, A.J., Stanier, P., Greene, N.D., 2013. Neural tube defects: recent advances, unsolved questions, and controversies. The Lancet Neurology 12, 799–810. https://doi.org/10.1016/S1474-4422(13)70110-8.
Cotti, S., Huysseune, A., Koppe, W., Rücklin, M., Marone, F., Wölfel, E.M., Fiedler, I.A., Busse, B., Forlino, A., Witten, P.E., 2020. More bone with less minerals? The effects of dietary phosphorus on the post-cranial skeleton in zebrafish. Int. J. Mol. Sci. 21, 5429. https://doi.org/10.3390/ijms21155429.
Cox, K.D., Covernton, G.A., Davies, H.L., Dower, J.F., Juanes, F., Dudas, S.E., 2019. Human consumption of microplastics. Environ. Sci. Technol. 53, 7068–7074.
Creuzet, S.E., 2009. Regulation of pre-otic brain development by the cephalic neural crest. Proc. Nat. Acad. Sci. 106, 15774–15779. https://doi.org/10.1073/pnas.0906072106.
Creuzet, S.E., Martinez, S., Le Douarin, N.M., 2006. The cephalic neural crest exerts a critical effect on forebrain and midbrain development. Proc Natl Acad Sci USA 103, 14033–14038. https://doi.org/10.1073/pnas.0605899103.
Dady, A., Blavet, C., Duband, J.L., 2012. Timing and kinetics of E- to N-cadherin switch during neurulation in the avian embryo. Dev Dyn 241, 1333–1349. https://doi.org/10.1002/dvdy.23813.
Dady, A., Havis, E., Escriou, V., Catala, M., Duband, J.L., 2014. Junctional neurulation: a unique developmental program shaping a discrete region of the spinal cord highly susceptible to neural tube defects. J Neurosci 34, 13208–13221. https://doi.org/10.1523/JNEUROSCI.1850-14.2014.
de Bakker, M.A.; Fowler, D.A.; Oude, K.d.; Dondorp, E.M.; Navas, M.; Horbanczuk, J.O.; Sire, J.-Y.; Szczerbińska, D.; Richardson, M.K. Digit loss in archosaur evolution and the interplay between selection and constraints. Nature 2013; 500: 445-448, 10.1038/nature12336. Epub 2013 Jul 7.
de Bakker, M.A.G., van der Vos, W., de Jager, K., Chung, W.Y., Fowler, D.A., Dondorp, E., Spiekman, S.N.F., Chew, K.Y., Xie, B., Jiménez, R., Bickelmann, C., Kuratani, S., Blazek, R., Kondrashov, P., Renfree, M.B., Richardson, M.K., 2021. Selection on Phalanx Development in the Evolution of the Bird Wing. Mol Biol Evol 38, 4222–4237. https://doi.org/10.1093/molbev/msab150.
Desai, S.B., Galage, C., 2015. Production and analysis of pyrolysis oil from waste plastic in Kolhapur city. Int. J. Eng. Res. Gen. Sci. 3, 590–595.
Erhardt, S., Zheng, M., Zhao, X., Le, T.P., Findley, T.O., Wang, J., 2021. The Cardiac Neural Crest Cells in Heart Development and Congenital Heart Defects. J Cardiovasc Dev Dis 2021;810.3390/jcdd8080089.
Escot, S., Blavet, C., Faure, E., Zaffran, S., Duband, J.L., Fournier-Thibault, C., 2016. Disruption of CXCR4 signaling in pharyngeal neural crest cells causes DiGeorge syndrome-like malformations. Development 143, 582–588. https://doi.org/10.1242/dev.126573.
Geetha-Loganathan, P., Nimmagadda, S., Hafez, I., Fu, K., Cullis, P.R., Richman, J.M., 2011. Development of high-concentration lipoplexes for in vivo gene function studies in vertebrate embryos. Dev. Dyn. 240, 2108–2119. https://doi.org/10.1002/dvdy.22708.
Gestri, G., Osborne, R.J., Wyatt, A.W., Gerrelli, D., Gribble, S., Stewart, H., Fryer, A., Bunyan, D.J., Prescott, K., Collin, J.R., Fitzgerald, T., Robinson, D., Carter, N.P., Wilson, S.W., Ragge, N.K., 2009. Reduced TFAP2A function causes variable optic fissure closure and retinal defects and sensitizes eye development to mutations in other morphogenetic regulators. Hum Genet 126, 791–803. https://doi.org/10.1007/s00439-009-0730-x.
Gibb, B.C., 2019. Plastics are forever. Nat Chem 11, 394–395. https://doi.org/10.1038/s41557-019-0260-7.
Gittenberger-de Groot, A.C., Winter, E.M., Bartelings, M.M., Goumans, M.J., DeRuiter, M.C., Poelmann, R.E., 2012. The arterial and cardiac epicardium in development, disease and repair. Differentiation 84, 41–53. https://doi.org/10.1016/j.diff.2012.05.002.
Gondré-Lewis, M.C., Gboluaje, T., Reid, S.N., Lin, S., Wang, P., Green, W., Diogo, R., Fidélia-Lambert, M.N., Herman, M.M., 2015. The human brain and face: mechanisms of cranial, neurological and facial development revealed through malformations of holoprosencephaly, cyclopia and aberrations in chromosome 18. J Anat 227, 255–267. https://doi.org/10.1111/joa.12343.
Gopinath, P.M., Saranya, V., Vijayakumar, S., Mythili Meera, M., Ruprekha, S., Kunal, R., Pranay, A., Thomas, J., Mukherjee, A., Chandrasekaran, N., 2019. Assessment on interactive prospectives of nanoplastics with plasma proteins and the toxicological impacts of virgin, coronated and environmentally released-nanoplastics. Sci Rep 9, 8860. https://doi.org/10.1038/s41598-019-45139-6.
Gourmelon, G., 2015. Global plastic production rises, recycling lags. Vital Signs 22, 91–95.
Green, S.A., Simoes-Costa, M., Bronner, M.E., 2015. Evolution of vertebrates as viewed from the crest. Nature 520, 474–482. https://doi.org/10.1038/nature14436.
Grocott, T., Johnson, S., Bailey, A.P., Streit, A., 2011. Neural crest cells organize the eye via TGF-beta and canonical Wnt signalling. Nat Commun 2, 265. https://doi.org/10.1038/ncomms1269.
Hamburger, V., Hamilton, H.L., 1951. A series of normal stages in the development of the chick embryo. J Morphol 88, 49–92.
Hollóczki, O., Gehrke, S., 2019. Nanoplastics can change the secondary structure of proteins. Sci. Rep. 9, 16013. https://doi.org/10.1038/s41598-019-52495-w.
Hutson, M.R., Kirby, M.L., 2007. Model systems for the study of heart development and disease. Cardiac neural crest and conotruncal malformations. Semin Cell Dev Biol 18, 101–110. https://doi.org/10.1016/j.semcdb.2006.12.004.
Jenner, L.C., Rotchell, J.M., Bennett, R.T., Cowen, M., Tentzeris, V., Sadofsky, L.R., 2022. Detection of microplastics in human lung tissue using muFTIR spectroscopy. Sci Total Environ 831, 154907. https://doi.org/10.1016/j.scitotenv.2022.154907.
Keibel, F., Abraham, K., 1900. Normentafeln zur Entwicklungsgeschichte des Huhnes (Gallus domesticus). In: Keibel, F. (Ed.), Normentafeln Zur Entwicklungsgeschichte Der Wirbelthiere. Fischer, Jena.
Keyte, A., Hutson, M.R., 2012. The neural crest in cardiac congenital anomalies. Differentiation 84, 25–40. https://doi.org/10.1016/j.diff.2012.04.005.
Kihara, S., Ashenden, A., Kaur, M., Glasson, J., Ghosh, S., van der Heijden, N., Brooks, A. E., Mata, J.P., Holt, S., Domigan, L.J., 2021. Cellular interactions with polystyrene nanoplastics—The role of particle size and protein corona. Biointerphases 16, 041001.
Kirby, M.L., 1999. 11 - Contribution of Neural Crest to Heart and Vessel Morphology. In: Harvey, R.P., Rosenthal, N. (Eds.), Heart Development. Academic Press, San Diego.
Kirby, M.L., Tumage, K.L., Hays, B.M., 1985. Characterization of conotruncal malformations following ablation of cardiac neural crest. Anat. Rec. 213, 87. https://doi.org/10.1002/ar.1092130112.
Kirby, M.L., Creazzo, T.L., Christiansen, J.L., 1989. Chronotropic responses of chick atria to field stimulation after various neural crest ablations. Circ Res 65, 1547–1554. https://doi.org/10.1161/01.res.65.6.1547.
Kirby, M.L., Waldo, K.L., 1995. Neural crest and cardiovascular patterning. Circ Res 77, 211–215. https://doi.org/10.1161/01.res.77.2.211.
Knezevic, V., De Santo, R., Mackem, S., 1998. Continuing organizer function during chick tail development. Development 125, 1791–1801. https://doi.org/10.1242/dev.125.10.1791.
Koelmans, A.A., Nor, N.H.M., Hermsen, E., Kooi, M., Mintenig, S.M., De France, J., 2019. Microplastics in freshwaters and drinking water: Critical review and assessment of data quality. Water Res. https://doi.org/10.1016/j.watres.2019.02.054.
Kögel, T., Bjorøy, Ø., Toto, B., Bienfait, A.M., Sanden, M., 2020. Micro-and nanoplastic toxicity on aquatic life: Determining factors. Sci. Total Environ. 709, 136050. https://doi.org/10.1016/j.scitotenv.2019.136050.
Kohl, A., Golan, N., Cinnamon, Y., Genin, O., Chefetz, B., Sela-Donenfeld, D., 2019. A proof of concept study demonstrating that environmental levels of carbamazepine impair early stages of chick embryonic development. Environ. Int. 129, 583–594. https://doi.org/10.1016/j.envint.2019.03.064.
Le Douarin, N.M., Couly, G., Creuzet, S.E., 2012. The neural crest is a powerful regulator of pre-otic brain development. Dev Biol 366, 74–82. https://doi.org/10.1016/j.ydbio.2012.01.007.
Le Douarin, N.M., Kalcheim, C., 1999. The Neural Crest. Cambridge University Press, Cambridge.
Lee, W.S., Cho, H.-J., Kim, E., Huh, Y.H., Kim, H.-J., Kim, B., Kang, T., Lee, J.-S., Jeong, J., 2019. Bioaccumulation of polystyrene nanoplastics and their effect on the toxicity of Au ions in zebrafish embryos. Nanoscale 11, 3173–3185. https://doi.org/10.1039/C8NR09321K.
Leslie, H.A., van Velzen, M.J.M., Brandsma, S.H., Vethaak, A.D., Garcia-Vallejo, J.J., Lamoree, M.H., 2022. Discovery and quantification of plastic particle pollution in human blood. Environ Int 163, 107199. https://doi.org/10.1016/j.envint.2022.107199.
Levine, B., Berman, W.E., 1995. The current status of expanded polytetrafluoroethylene (Gore-Tex) in facial plastic surgery. Ear, Nose Throat J. 74, 681–684.
Malik, R., Zilberman, M.V., Tang, L., Miller, S., Pandian, N.G., 2015. Ectopia cordis with a double outlet right ventricle, large ventricular septal defect, malposed great arteries and left ventricular hypoplasia. Echocardiography 32, 589–591. https://doi.org/10.1111/echo.12843.
Marone, F., Studer, A., Billich, H., Sala, L., Stampanoni, M., 2017. Towards on-the-fly data post-processing for real-time tomographic imaging at TOMCAT. Adv. Struct. Chem. Imag. 3, 1–11. https://doi.org/10.1186/s40679-016-0035-9.
Martik, M.L., Bronner, M.E., 2021. Riding the crest to get a head: neural crest evolution in vertebrates. Nat Rev Neurosci 22, 616–626. https://doi.org/10.1038/s41583-021-00503-2.
McClelland, K.S., Ng, E.T., Bowles, J., 2016. Agarose/gelatin immobilisation of tissues or embryo segments for orientated paraffin embedding and sectioning. Differentiation 91, 68–71. https://doi.org/10.1016/j.diff.2015.12.001.
McDonald-McGinn, D.M., Sullivan, K.E., 2011. Chromosome 22q11.2 deletion syndrome (DiGeorge syndrome/velocardiofacial syndrome). Medicine (Baltimore) 90, 1–18. https://doi.org/10.1097/MD.0b013e3182060469.
Metscher, B.D., 2009. MicroCT for developmental biology: A versatile tool for high-contrast 3D imaging at histological resolutions. Dev Dynam: Off Publ Am Assoc Anatom 238, 632–640. https://doi.org/10.1186/1472-6793-9-11.
Newbern, J., Zhong, J., Wickramasinghe, R.S., Li, X., Wu, Y., Samuels, I., Cherosky, N., Karlo, J.C., O'Loughlin, B., Wikenheiser, J., Gargesha, M., Doughman, Y.Q., Charron, J., Ginty, D.D., Watanabe, M., Saitta, S.C., Snider, W.D., Landreth, G.E., 2008. Mouse and human phenotypes indicate a critical conserved role for ERK2 signaling in neural crest development. Proc Natl Acad Sci U S A 105, 17115–17120. https://doi.org/10.1073/pnas.0805239105.
Nie, J.-H., Shen, Y., Roshdy, M., Cheng, X., Wang, G., Yang, X., 2021. Polystyrene nanoplastics exposure caused defective neural tube morphogenesis through caveolae-mediated endocytosis and faulty apoptosis. Nanotoxicology 1–20. https://doi.org/10.1080/17435390.2021.1930228.
Paganin, D., Mayo, S.C., Gureyev, T.E., Miller, P.R., Wilkins, S.W., 2002. Simultaneous phase and amplitude extraction from a single defocused image of a homogeneous object. J. Microsc. 206, 33–40. https://doi.org/10.1046/j.1365-2818.2002.01010.x.
Panda, A.K., Singh, R.K., Mishra, D., 2010. Thermolysis of waste plastics to liquid fuel: A suitable method for plastic waste management and manufacture of value added products—A world prospective. Renew. Sustain. Energy Rev. 14, 233–248. https://doi.org/10.1016/j.rser.2009.07.005.

Pitt, J.A., Trevisan, R., Massarsky, A., Kozal, J.S., Levin, E.D., Di Giulio, R.T., 2018. Maternal transfer of nanoplastics to offspring in zebrafish (Danio rerio): A case study with nanopolystyrene. Sci Total Environ 643, 324–334. https://doi.org/10.1016/j.scitotenv.2018.06.186.

Platt, D.K., 2003. Engineering and high performance plastics market report: a Rapra market report ed^eds. iSmithers Rapra Publishing.

Poelmann, R.E., Mikawa, T., Gittenberger-de Groot, A.C., 1998. Neural crest cells in outflow tract septation of the embryonic chicken heart: differentiation and apoptosis. Dev Dyn 212, 373–384. https://doi.org/10.1002/(SICI)1097-0177(199807)212:3<373::AID-AJA5>3.0.CO;2-E.

Porras, D., Brown, C.B., 2008. Temporal-spatial ablation of neural crest in the mouse results in cardiovascular defects. Dev Dyn 237, 153–162. https://doi.org/10.1002/dvdy.21382.

Ragusa, A., Svelato, A., Santacroce, C., Catalano, P., Notarstefano, V., Carnevali, O., Papa, F., Rongioletti, M.C.A., Baiocco, F., Draghi, S., Plasticenta: First evidence of microplastics in human placenta. Environment International 146:106274-106274, 10.1016/j.envint.2020.106274.

Röcker, C., Pötzl, M., Zhang, F., Parak, W.J., Nienhaus, G.U., 2009. A quantitative fluorescence study of protein monolayer formation on colloidal nanoparticles. Nat. Nanotechnol. 4, 577–580.

Seller, M.J., 1995. Sex, neural tube defects, and multisite closure of the human neural tube. Am J Med Genet 58, 332–336. https://doi.org/10.1002/ajmg.1320580406.

Shook, D., Keller, R., 2003. Mechanisms, mechanics and function of epithelial-mesenchymal transitions in early development. Mech Dev 120, 1351–1383. https://doi.org/10.1016/j.mod.2003.06.005.

Silver, P. Special problems of experimenting in ovo on the early chick embryo, and a solution. 1960;10.1242/dev.8.4.369.

Smits-van Prooije, A.E., Poelmann, R.E., Gesink, A.F., van Groeningen, M.J., Vermeij-Keers, C., 1986. The cell surface coat in neurulating mouse and rat embryos, studied with lectins. Anat Embryol (Berl) 175, 111–117. https://doi.org/10.1007/BF00315461.

Snarr, B.S., Kern, C.B., Wessels, A., 2008. Origin and fate of cardiac mesenchyme. Dev Dyn 237, 2804–2819. https://doi.org/10.1002/dvdy.21725.

Sridharan, S., Kumar, M., Saha, M., Kirkham, M.B., Singh, L., Bolan, N.S., 2022. The polymers and their additives in particulate plastics: What makes them hazardous to the fauna? Sci. Total Environ. 824, 153828.

Stampanoni, M.; Groso, A.; Isenegger, A.; Mikuljan, G.; Chen, Q.; Bertrand, A.; Henein, S.; Betemps, R.; Frommherz, U.; Böhler, P. Trends in synchrotron-based tomographic imaging: the SLS experience. Developments in X-ray Tomography V: International Society for Optics and Photonics; 2006, 10.1117/12.679497.

Subramanian, P., 2000. Plastics recycling and waste management in the US. Resour. Conserv. Recycl. 28, 253–263.

Taneyhill, L.A.; Schiffmacher, A.T. Should I stay or should I go? Cadherin function and regulation in the neural crest. Genesis 2017;5510.1002/dvg.23028.

Verma, A.S., Fitzpatrick, D.R., 2007. Anophthalmia and microphthalmia. Orphanet J Rare Dis 2, 47. https://doi.org/10.1186/1750-1172-2-47.

Vighi, M., Bayo, J., Fernández-Piñas, F., Gago, J., Gómez, M., Hernández-Borges, J., Herrera, A., Landaburu, J., Muniategui-Lorenzo, S., Muñoz, A.-R., 2021. Micro and nano-plastics in the environment: research priorities for the near future. Rev. Environ. Contam. Toxicol. 257, 163–218. https://doi.org/10.1117/12.679497.

Waldo, K., Miyagawa-Tomita, S., Kumiski, D., Kirby, M.L., 1998. Cardiac neural crest cells provide new insight into septation of the cardiac outflow tract: aortic sac to ventricular septal closure. DevBiol 196, 129–144. https://doi.org/10.1006/dbio.1998.8860.

Waldo, K., Zdanowicz, M., Burch, J., Kumiski, D.H., Stadt, H.A., Godt, R.E., Creazzo, T.L., Kirby, M.L., 1999. A novel role for cardiac neural crest in heart development. J Clin Invest 103, 1499–1507. https://doi.org/10.1172/jci6501.

Webb, H.K., Arnott, J., Crawford, R.J., Ivanova, E.P., 2012. Plastic degradation and its environmental implications with special reference to poly (ethylene terephthalate). Polymers 5, 1–18. https://doi.org/10.3390/polym5010001.

Weigele, J.; Bohnsack, B.L. Genetics Underlying the Interactions between Neural Crest Cells and Eye Development. J Dev Biol 2020;810.3390/jdb8040026.

Yan, Y., Wang, G., Huang, J., Zhang, Y., Cheng, X., Chuai, M., Brand-Saberi, B., Chen, G., Jiang, X., Yang, X., 2020. Zinc oxide nanoparticles exposure-induced oxidative stress restricts cranial neural crest development during chicken embryogenesis. Ecotoxicol Environ Saf 194, 110415. https://doi.org/10.1016/j.ecoenv.2020.110415.

Yi, W., Rücklin, M., Poelmann, R.E., Aldridge, D.C., Richardson, M.K., 2021. Normal stages of embryonic development of a brood parasite, the rosy bitterling Rhodeus ocellatus (Teleostei: Cypriniformes). J. Morphol. 282, 783–819. https://doi.org/10.1002/jmor.21335.

Yong, C.Q.Y.; Valiyaveettil, S.; Tang, B.L. Toxicity of Microplastics and Nanoplastics in Mammalian Systems. Int J Environ Res Public Health 2020;1710.3390/ijerph17051509.

Zhang, J., Wang, L., Kannan, K., 2020. Microplastics in house dust from 12 countries and associated human exposure. Environ. Int. 134, 105314 https://doi.org/10.1016/j.envint.2019.105314.

Zhao, L., Qu, M., Wong, G., Wang, D., 2017. Transgenerational toxicity of nanopolystyrene particles in the range of μg L− 1 in the nematode Caenorhabditis elegans. Environ. Sci. Nano 4, 2356–2366. https://doi.org/10.1016/j.envpol.2019.113122.